Caveolae regulate the nanoscale organization of the plasma membrane to remotely control Ras signaling

Nicholas Ariotti,[1] Manuel A. Fernández-Rojo,[1] Yong Zhou,[2] Michelle M. Hill,[1] Travis L. Rodkey,[2] Kerry L. Inder,[1] Lukas B. Tanner,[3] Markus R. Wenk,[3] John F. Hancock,[2] and Robert G. Parton[1]

[1]The University of Queensland, Institute for Molecular Bioscience, Queensland 4072, Australia
[2]Department of Integrative Biology and Pharmacology, The University of Texas Medical School-Houston, Houston, TX 77030
[3]Department of Biochemistry, Yong Loo Lin School of Medicine, National University of Singapore, Centre for Life Sciences, 117456 Singapore

The molecular mechanisms whereby caveolae exert control over cellular signaling have to date remained elusive. We have therefore explored the role caveolae play in modulating Ras signaling. Lipidomic and gene array analyses revealed that caveolin-1 (CAV1) deficiency results in altered cellular lipid composition, and plasma membrane (PM) phosphatidylserine distribution. These changes correlated with increased K-Ras expression and extensive isoform-specific perturbation of Ras spatial organization: in CAV1-deficient cells K-RasG12V nanoclustering and MAPK activation were enhanced, whereas GTP-dependent lateral segregation of H-Ras was abolished resulting in compromised signal output from H-RasG12V nanoclusters. These changes in Ras nanoclustering were phenocopied by the down-regulation of Cavin1, another crucial caveolar structural component, and by acute loss of caveolae in response to increased osmotic pressure. Thus, we postulate that caveolae remotely regulate Ras nanoclustering and signal transduction by controlling PM organization. Similarly, caveolae transduce mechanical stress into PM lipid alterations that, in turn, modulate Ras PM organization.

Introduction

Caveolae are 50–80-nm bulb-shaped plasma membrane (PM) microdomains enriched in cholesterol and glycosphingolipids (Ortegren et al., 2004). Many studies have implicated caveolin-1 (CAV1), the major structural protein of caveolae (Rothberg et al., 1992), in the regulation of key cellular signaling cascades. EGF-mediated activation of the MAPK cascade is dependent on CAV1 expression (Engelman et al., 1998; Galbiati et al., 1998) and CAV1 is known to regulate Src-family kinases, receptor tyrosine kinases, and eNOS (García-Cardeña et al., 1996; Li et al., 1996; Couet et al., 1997). One hypothesis for these diverse regulatory effects is that direct binding of CAV1 inhibits the activity of the cognate signaling molecule (García-Cardeña et al., 1996; Couet et al., 1997). However, the predicted extensive enrichment of this large set of signaling molecules within caveolae by this mechanism has not been validated by EM analysis (Prior et al., 2003a; Hancock and Prior, 2005; Plowman et al., 2005). Furthermore, a recent structural analysis of proposed interacting signaling proteins showed that the putative binding motif for CAV1 is inaccessible such that CAV1 could not function as a direct allosteric regulator (Collins et al., 2012). Thus, CAV1 and caveolae likely regulate cellular signaling cascades by an alternate mechanism.

Loss of CAV1 has diverse consequences for membrane organization and dynamics. Mobility of lipid components is altered dependent on CAV1 expression, ordered domains are less abundant, and accelerated endocytosis has been observed in caveolin-deficient cells (Gaus et al., 2006; Hernández-Deviez et al., 2008; Hoffmann et al., 2010). CAV1 can bind cholesterol and cholesterol depletion affects both CAV1 expression and the

N. Ariotti and M.A. Fernández-Rojo contributed equally to this paper.

Correspondence to Robert G. Parton: r.parton@imb.uq.edu; or John F. Hancock: john.f.hancock@uth.tmc.edu

M.M. Hill's and K.L. Inder's present address is The University of Queensland, Diamantina Institute, Queensland 4102, Australia.

Abbreviations used in this paper: AML12, alpha mouse liver 12; BHK, baby hamster kidney; CAV, caveolin; FLIM, fluorescence lifetime imaging microscopy; FRET, fluorescence resonance energy transfer; GM3, ganglioside monosialodihexosylganglioside; HG12V, H-RasG12V; kd, knockdown; KG12V, K-RasG12V; L_o, liquid ordered; MβCD, methyl-β-cyclodextrin; MEF, mouse embryonic fibroblast; PC, phosphatidylcholine; PE, phosphatidylethanolamine; PI, phosphatidylinositol; PM, plasma membrane; PS, phosphatidylserine; SL, sphingolipid; SM, sphingomyelin; WT, wild type.

© 2014 Ariotti et al. This article is distributed under the terms of an Attribution–Noncommercial–Share Alike–No Mirror Sites license for the first six months after the publication date (see http://www.rupress.org/terms). After six months it is available under a Creative Commons License (Attribution–Noncommercial–Share Alike 3.0 Unported license, as described at http://creativecommons.org/licenses/by-nc-sa/3.0/).

The Rockefeller University Press $30.00
J. Cell Biol. Vol. 204 No. 5 777–792
www.jcb.org/cgi/doi/10.1083/jcb.201307055

THE JOURNAL OF CELL BIOLOGY

Downloaded from http://rupress.org/jcb/article-pdf/204/5/777/1583044/jcb_201307055.pdf by guest on 24 April 2024

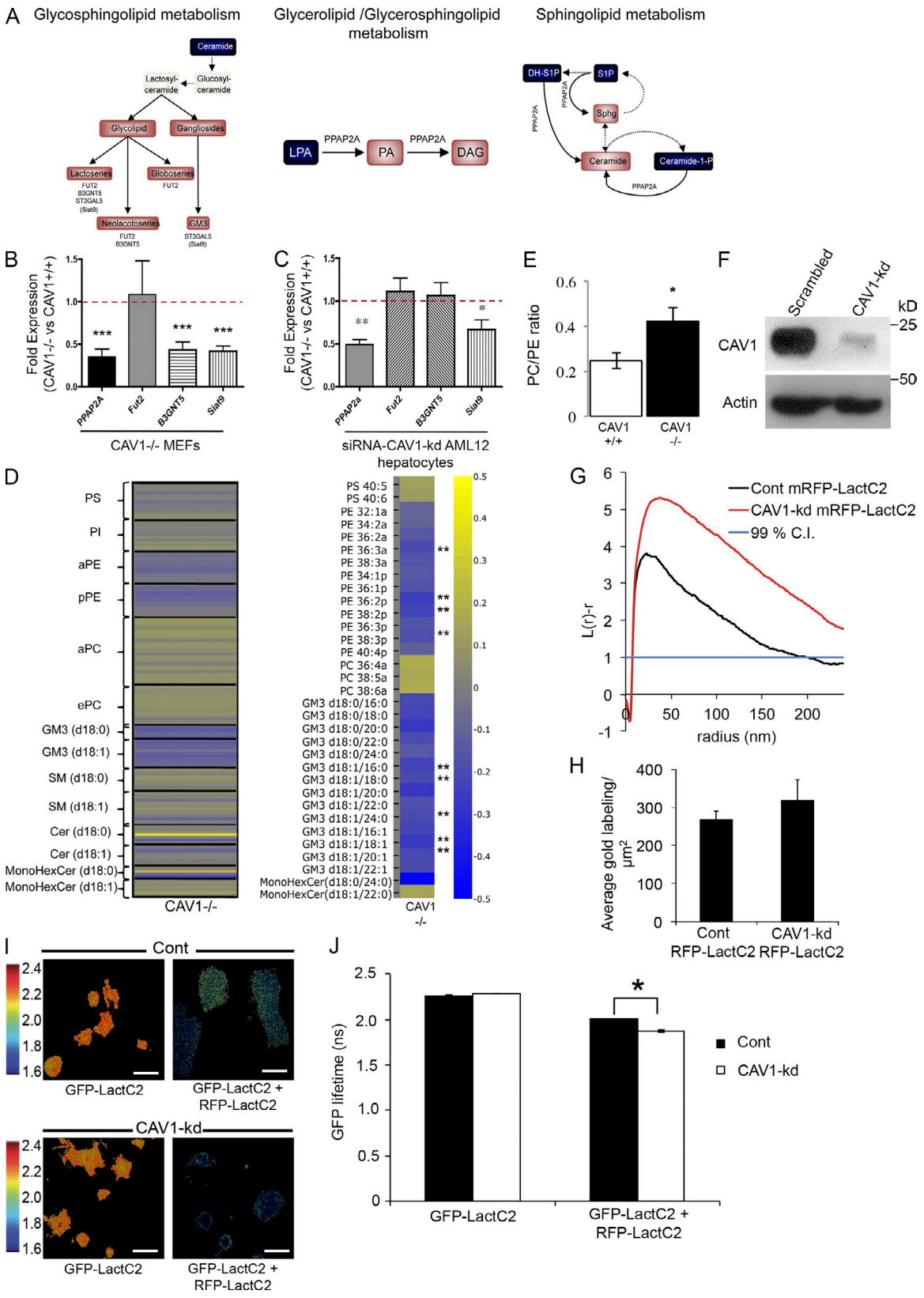

Figure 1. **CAV1 deficiency impairs glycosphingolipid and glycerolipid synthesis, levels, and distribution.** (A) Lipid metabolism gene pathways affected by CAV1 deficiency in MEFs (adapted from Kyoto Encyclopedia of Genes and Genomes; http://www.genome.jp/kegg). (B) Reduced expression of Ppap2A, B3GNT5, and Siat9 in CAV1$^{-/-}$ MEFs (n = 5). (C) siRNA-CAV1 knockdown in AML12 hepatocytes decreased Siat9 and Ppap2A expression (n = 4). (D, left) Heat-plot representing global changes to lipid species (decreased lipids colored blue and increased lipids colored yellow) in CAV1$^{-/-}$ MEFs relative to the average value obtained from CAV1$^{+/+}$ MEFs. Values are relative to internal standards and the total amount of lipids: heat plots are represented as a ratio of log (KO/WT). (Right) Expanded heat-plot representing lipid species that were significantly affected ($P < 0.05$) in the CAV1$^{-/-}$ MEFs relative to CAV1$^{+/+}$

Downloaded from http://rupress.org/jcb/article-pdf/204/5/777/1583044/jcb_201307055.pdf by guest on 24 April 2024

structural integrity of caveolae (Rothberg et al., 1992; Murata et al., 1995; Ortegren et al., 2004). Other studies have linked specific lipid species to CAV1. Expression of the ganglioside monosialodihexosylganglioside (GM3) synthase causes up-regulation of CAV1 (Prinetti et al., 2010), and CAV1 localization to the PM can be altered by addition of exogenous GM3 (Wang et al., 2002). These data suggest that caveolae may function as liquid-ordered storage centers that sequester specific lipids and control key membrane properties such as fluidity (Parton and Simons, 2007). In this context, given that lipid-based sorting is a fundamental principle underlying the organization of the cell surface that is especially relevant to the assembly of functional signaling complexes (Lingwood and Simons, 2010), caveolae may regulate signal transmission by controlling the lipid composition of the PM.

To further elucidate the role of caveolae in signal transduction we have combined loss or down-regulation of key caveolar components with an analysis of Ras signal transmission. H-, N-, and K-Ras are lipid-anchored GTPases that operate as molecular switches to regulate cell growth, proliferation, and differentiation (Hancock, 2003). The nanoscale spatial organization of Ras on the PM is essential for effective signal transmission. Specifically, Ras proteins are distributed heterogeneously over the PM in a combination of immobile nanoclusters and freely diffusing monomers (Hancock and Parton, 2005). A nanocluster comprises ~7 Ras proteins, has a radius of ~9 nm, and an estimated lifetime of 0.5–1 s (Murakoshi et al., 2004; Plowman et al., 2005). The term nanocluster captures the concept that Ras proteins drive the formation of their cognate nanoscale environments. Key Ras determinants for nanocluster formation include the C-terminal membrane anchor, the hyper-variable linker region adjacent to the anchor, and G-domain activation state (Rotblat et al., 2004; Abankwa et al., 2007, 2008; Gorfe et al., 2007). In consequence, H- and K-Ras assemble into spatially nonoverlapping nanoclusters with further lateral segregation into nonoverlapping GDP and GTP nanoclusters (Prior et al., 2003a; Plowman et al., 2005, 2008; Roy et al., 2005; Zhou et al., 2012). H-Ras associates with cholesterol-dependent nanoclusters on the inner leaflet of the PM when in an inactive GDP-bound state and, upon GTP loading, switches to cholesterol-insensitive nanodomains; K-Ras occupies cholesterol-insensitive nanoclusters in both GTP- and GDP-bound states that have been closely linked with phosphatidylserine (PS; Cho et al., 2012; van der Hoeven et al., 2013). Ras.GTP nanoclusters are the sole sites of effector recruitment and activation on the PM (Hibino et al., 2003; Murakoshi et al., 2004; Tian et al., 2007; Plowman et al., 2008), such that Ras signal transmission is abrogated if nanoclustering is inhibited, or nanocluster structure is perturbed (Plowman et al., 2005; Tian et al., 2007; Cho et al., 2012; Zhou et al., 2012; van der Hoeven et al., 2013).

Previous work has shown that expression of dominant-negative or mutant CAV1 proteins selectively abrogate H-Ras but not K-Ras signal transmission (Roy et al., 1999; Carozzi et al., 2002). In the present study we have examined the consequences of loss of caveolae on specific Ras signaling pathways using $CAV1^{-/-}$ cells, cells with down-regulated CAV1 and Cavin1/polymerase transcript release factor (an essential structural component of caveolae) or an acute loss of caveolae by modulating cellular osmotic pressure. Using a range of techniques we now show that loss of caveolae perturbs Ras organization at the PM in an isoform-specific manner. We postulate that these changes are a direct result of alterations in the lipid profile and lipid organization of the PM as determined by comparative lipidomic profiling, by EM spatial analysis, and by fluorescence lifetime imaging microscopy combined with fluorescence resonance energy transfer (FLIM-FRET). These findings have wide-ranging implications for the role of CAV1 and caveolae in the control of PM lipid organization and in operation of lipid-based signaling assemblies. In addition, for the first time these studies link the lipid regulatory roles of caveolae with their mechanosensing activity.

Results

CAV1 deficiency is associated with changes in membrane lipid composition and organization

Signaling through H- and K-Ras isoforms is differentially sensitive to cholesterol depletion (Roy et al., 1999; Prior et al., 2001; Prior et al., 2003a). Cells transformed by either K-Ras or H-Ras also show altered ganglioside levels (Suzuki et al., 1989) and oncogenic K-Ras activity can be regulated by the levels of PM PS (Cho et al., 2012; van der Hoeven et al., 2013). We have previously analyzed changes in the expression of genes associated with lipid regulation comparing $CAV1^{+/+}$ and $CAV1^{-/-}$ mouse embryonic fibroblasts (MEFs). Our analysis showed the most significantly deregulated pathways were glycosphingolipid (GSL) and sphingolipid (SL) metabolism (Fernández-Rojo et al., 2013). CAV1 deficiency led to decreased expression of *Fut2* and *B3Gnt5* that participate in glycosphingolipid biosynthesis (Marcos et al., 2008; Magalhães et al., 2009), *ST3Gal5* (also known as *Siat9 or GM3 synthase*) involved in ganglioside biosynthesis (Yamashita et al., 2003), and *Ppap2A* (also known as *Lpp1*) that functions in sphingolipid, glycerolipid, and glycerophospholipid metabolism (Fernández-Rojo et al., 2013; the

MEFs (n = 6). The double asterisk denotes lipid species with a P-value < 0.01. (E) Ratio of abundance of PC to PE between $CAV1^{+/+}$ MEFs and $CAV1^{-/-}$ MEFs (n = 6). In B, C, and E the data represent the mean ± SEM, and for B–E statistical significance was determined by two-tailed Student's t test analyses. *, P < 0.05; **, P < 0.01; ***, P < 0.001. (F) Western blot demonstrating CAV1 protein levels between lentiviral shRNA-scrambled control BHK cells and shRNA-CAV1 knockdown BHK cells. (G) Down-regulation of CAV1 (red line) results in increased nanoclustering of PS (mRFP-LactC2) in BHK cells (Cont represents shScrambled—black line; n = 11 for control and n = 19 for CAV1-kd). Univariate analysis of spatial point patterns was conducted and statistical significance was determined by bootstrap analysis (P = 0.001). 99% confidence interval (C.I., light blue line) represents the threshold value at which sets of spatial point patterns are clustered. (H) Quantification of amount of gold labeling per 1 μm^2; equivalent levels of mRFP-LactC2 were observed on PM lawns derived from control and CAV1-kd BHK cells. (I) FLIM-FRET images of Cont and CAV1-kd BHK cells expressing either GFP-LactC2 alone or GFP-LactC2 and RFP-LactC2. (J) Quantification demonstrating an increase in the nanoclustering of PS represented by a significant reduction in GFP lifetime in CAV1-kd cells. The data are averaged (±SEM) from at least 60 whole-cell GFP lifetimes and statistical significance was determined using one-way ANOVA. Bar, 20 µm.

Downloaded from http://rupress.org/jcb/article-pdf/204/5/777/1583044/jcb_201307055.pdf by guest on 24 April 2024

role of these genes in lipid metabolism is depicted in Fig. 1 A; Pyne et al., 2004). We confirmed reduced expression of *B3Gnt5*, *Siat9*, and *Ppap2A* in CAV1$^{-/-}$ MEFs by qRT-PCR (Fig. 1 B). Reduced *Siat9* and *Ppap2A* expression was also recapitulated by transient siRNA-CAV1 knockdown (kd) in alpha mouse liver 12 (AML12) hepatocytes (Fig. 1 C).

To determine if these deregulated genes resulted in downstream changes to the cellular lipid profile, systematic high performance liquid chromatography (HPLC) and quantitative mass spectrometry (MS)–based analysis was performed comparing CAV1$^{+/+}$ and CAV1$^{-/-}$ MEFs. Our results demonstrated that GM3 cellular content was significantly lower in CAV1$^{-/-}$ MEFs (0.00322 ± 0.00024; mean ± SEM; values are relative to internal standards and total lipids from whole-cell preparations) than in CAV1$^{+/+}$ MEFs (0.00522 ± 0.00043; mean ± SEM, $P < 0.005$; Fig. 1 D and Fig. S1 A). GM3 is the major glycosphingolipid species in mammalian cells and the precursor of other minor glycosphingolipid species (Sandhoff and Kolter, 2003), and accordingly, the total glycosphingolipid content was also reduced in CAV1$^{-/-}$ MEFs (Fig. S1 B). Reduced GM3 cell content was accompanied by significant changes in specific but not in total cellular GM3 precursor levels, such as ceramides and monohexosyl ceramide species (glucosyl and lactosylceramides; Fig. 1 D). Lipidomic analysis also showed that CAV1$^{-/-}$ MEFs had alterations in glycerophospholipids, with a higher phosphatidylcholine (PC)/phosphatidylethanolamine (PE) ratio compared with CAV1$^{+/+}$ MEFs (Fig. 1, D and E; Fig. S1, B–D). CAV1$^{-/-}$ MEFs showed reduced levels of most PE species, a significant increase in three PC species, and a significant increase in specific long-chain PS species (Fig. 1 D and Fig. S1 D). Cholesterol levels were unchanged between CAV1$^{+/+}$ and CAV1$^{-/-}$ MEFs.

In view of the altered lipid profile of the CAV1$^{-/-}$ cells and the role of specific lipids in K-Ras membrane targeting and activity (Cho et al., 2012), we next investigated whether loss of CAV1 also affected the spatial distribution of PS at the PM. To do this we performed univariate spatial point pattern Ripley's K-function analysis on immunogold-labeled PM sheets; however, as MEFs are unsuitable for the preparation of PM lawns for spatial point pattern analyses, we generated stable shRNA-lentiviral (Sigma-Aldrich) knockdowns of CAV1 in the best characterized cell system for this approach—baby hamster kidney (BHK) cells. The CAV1-kd BHK cells demonstrated a significant reduction, ∼80%, in the level of CAV1 protein (Fig. 1 F). Ripley's K-function spatial point pattern analysis of PS was performed with control (shScrambled) and CAV1-kd BHK cells expressing mRFP-LactC2—a molecular probe that specifically associates with PS domains on the inner leaflet of the PM (Fairn et al., 2011; Kay et al., 2012). This analysis involves digitizing the spatial distributions of gold particles in a given region of interest (1 μm^2 of PM lawn) into a set of x and y coordinates. These positions are then analyzed relative to one another over a given radius and compared with distributions expected for complete spatial randomness (where L(r)-r = 0). An L(r)-r value above the 99% confidence interval demonstrates a nonrandom clustered distribution. Consistent with previous results, in wild-type (WT) cells we observed a nonrandom, clustered distribution of PS (Fairn et al., 2011; Cho et al., 2012; van der Hoeven et al., 2013). In CAV1-kd cells the extent of PS clustering was dramatically increased (Fig. 1 G) without altering the level of mRFP-LactC2 at the PM (Fig. 1 H). These observations were confirmed by FLIM-FRET analysis of BHK cells cotransfected with GFP and RFP-tagged LactC2. The significant reduction in GFP lifetime in the CAV1-kd cells is indicative of a closer spatial relationship between differentially tagged LactC2 fusion proteins and therefore increased nanoclustering. This suggests that while the PS content of the inner leaflet is unchanged by CAV1 depletion, a substantial reorganization of PS domains occurs. Therefore, CAV1 modulates cellular glycosphingolipid, sphingolipid, and glycerophospholipid metabolism resulting in profound effects on cellular lipid content, and regulates the spatial organization of lipid species on the inner leaflet of the PM.

Down-regulation of CAV1 causes an extensive reorganization of Ras nanoclusters

Given that Ras nanoclusters are transient, lipid-based assemblies, the observed changes in the lipid composition and organization of the PM induced by CAV1 loss would be expected to have significant consequences for Ras spatial organization. We therefore surveyed the distribution of different Ras isoforms using PM sheets prepared from K-Ras–expressing control (shScrambled) and CAV1-kd BHK cells. We observed major differences in Ras nanoclustering dependent on CAV1 expression. Clustering of GFP-tK (the minimal membrane anchor of K-Ras) was significantly higher in CAV1-kd cells compared with control cells. This effect was rescued by caveolin-3 (CAV3) expression (Fig. 2 A). These observations were confirmed with FLIM-FRET analysis—a significant reduction in the GFP lifetime of CAV1-kd cells expressing GFP- and RFP-tagged tK was observed when compared with control cells (Fig. 2 B). Identical results were observed with the nanoclustering of GFP-K-RasG12V (K-Ras.GTP; Fig. 2, C and D) and full-length GFP-K-RasWT (K-Ras.GDP; Fig. S2 A).

Changes to H-Ras spatial organization were more extensive. Clustering of GFP-tH (the minimal membrane anchor of H-Ras) was significantly lower in CAV1-kd cells compared with control cells (Fig. 3 A). This reduction in nanoclustering was rescued by expressing CAV3-mHA (Fig. 3 A). Mirroring this observation, full-length GFP-H-RasWT (H-Ras.GDP) clustering was abrogated in CAV1-kd cells and rescued by CAV3 co-expression (Fig. S2 B). In contrast, no differences were observed to the nanoclustering profiles of control and CAV1-kd BHK cells expressing GFP-H-Ras.GTP (H-RasG12V; Fig. 3 B). To analyze if loss of CAV1 affects the lateral segregation of H-Ras, bivariate analysis of the co-clustering between H-Ras.GDP (tH) and H-Ras.GTP and FLIM-FRET was undertaken. Bivariate analysis measures the extent of colocalization of two different spatial point pattern populations (the $L_{biv}(r)$-r value directly correlates with the extent of co-clustering—at values greater than 1 the two different populations can be said to co-cluster). In WT cells H-Ras.GTP and H-Ras.GDP/RFP-tH laterally segregate into spatially nonoverlapping nanoclusters (Fig. 3, C and E). In contrast, extensive colocalization of GFP-H-Ras.GTP and RFP-tH was identified in CAV1-kd cells, indicating that H-Ras GTP-dependent segregation fails in the PM of CAV1-kd cells (Fig. 3, C and E). Furthermore, this effect was mimicked by depletion of

Downloaded from http://rupress.org/jcb/article-pdf/204/5/777/1583044/jcb_201307055.pdf by guest on 24 April 2024

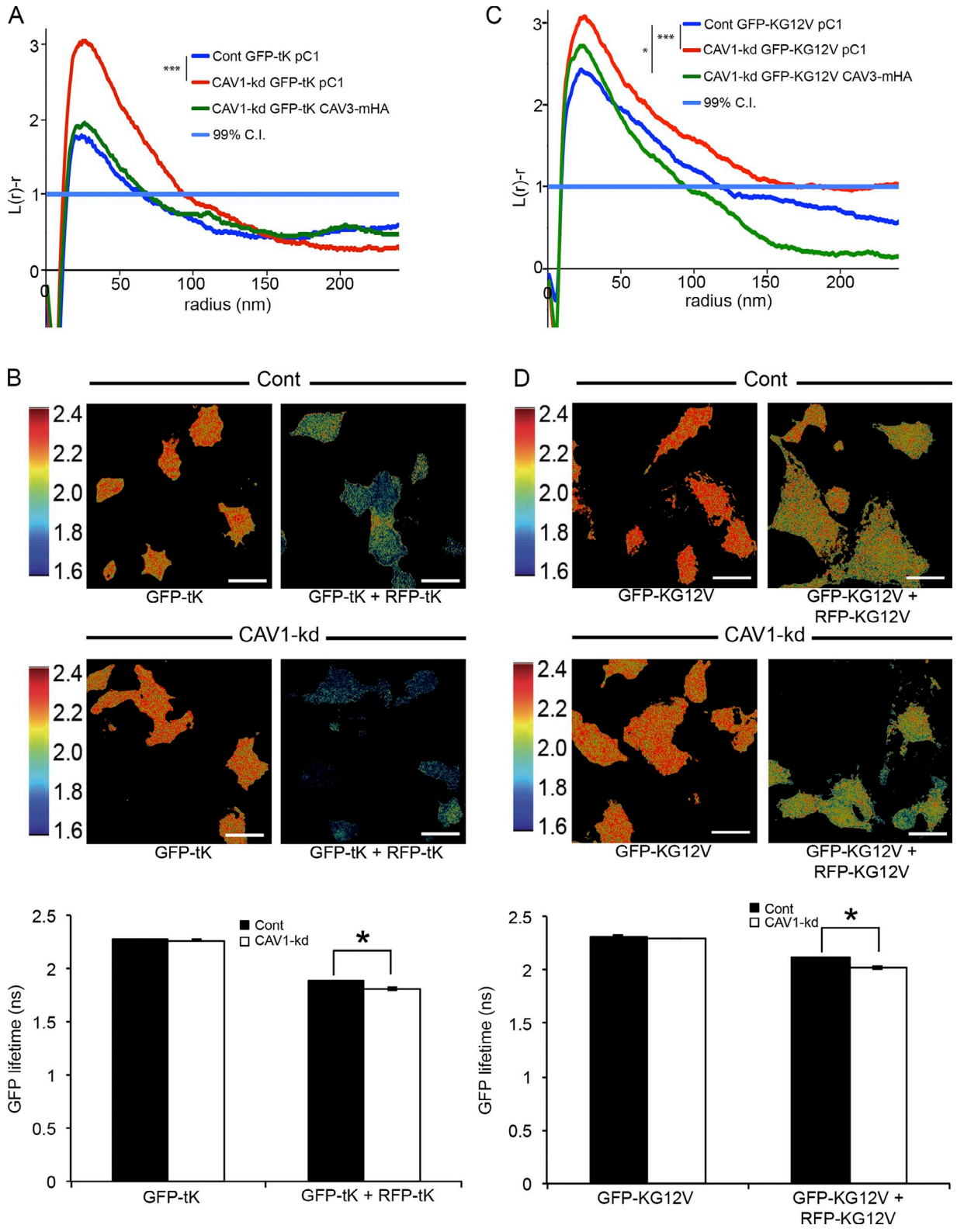

Figure 2. **Caveolin is essential for the regulation of K-Ras nanoclustering on the PM.** (A) PM sheets were prepared from cells expressing GFP-tK cotransfected with a control plasmid (empty vector, pC1) or CAV3-mHA (n = 11, n = 12, and n = 12 for control, CAV1-kd, and CAV1-kd + CAV3-mHA, respectively) and univariate spatial point pattern analysis. The nanoclustering of GFP-tK was increased in CAV1-kd cells compared with control, an effect that was rescued by expression of CAV3-mHA. (B) FLIM-FRET analysis of GFP-tK also demonstrated a significant increase in nanoclustering of tK in CAV1-kd cells compared with control. Bars, 20 µm. (C) GFP-K-RasG12V nanoclustering was similarly increased in CAV1-kd cells and was partially rescued toward control nanoclustering levels by CAV3-mHA expression (n = 9, n = 11, and n = 12 for control, CAV1-kd, and CAV1-kd + CAV3-mHA, respectively). (D) Increased nanoclustering of K-RasG12V was confirmed by FLIM-FRET analysis. Bars, 20 µm. Statistical significance was determined by bootstrap analysis for A and C (*, $P < 0.05$; ***, $P < 0.001$) and by one-way ANOVA for B and D.

Downloaded from http://rupress.org/jcb/article-pdf/204/5/777/1583044/jcb_201307055.pdf by guest on 24 April 2024

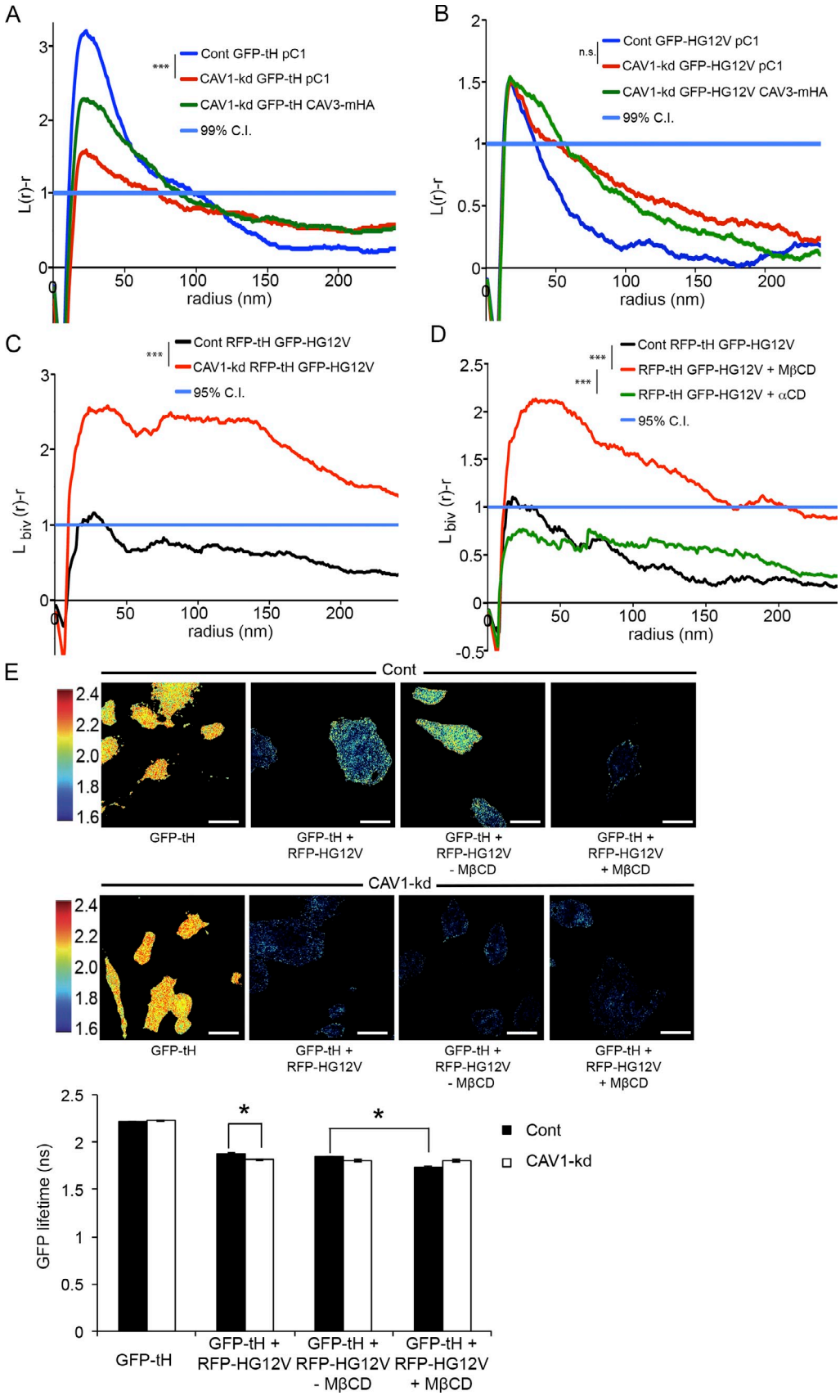

Figure 3. **Caveolin is essential for the correct lateral segregation of H-Ras on the PM.** PM sheets were prepared from cells expressing (A) GFP-tH or (B) GFP-H-RasG12V cotransfected with pC1 or CAV3-mHA (n = 12, n = 10, and n = 11 for control, CAV1-kd, and CAV1-kd + CAV3-mHA, respectively). (A) A significant decrease in nanoclustering of GFP-tH was observed in CAV1-kd cells when compared with control cells—an effect that was rescued by the

Downloaded from http://rupress.org/jcb/article-pdf/204/5/777/1583044/jcb_201307055.pdf by guest on 24 April 2024

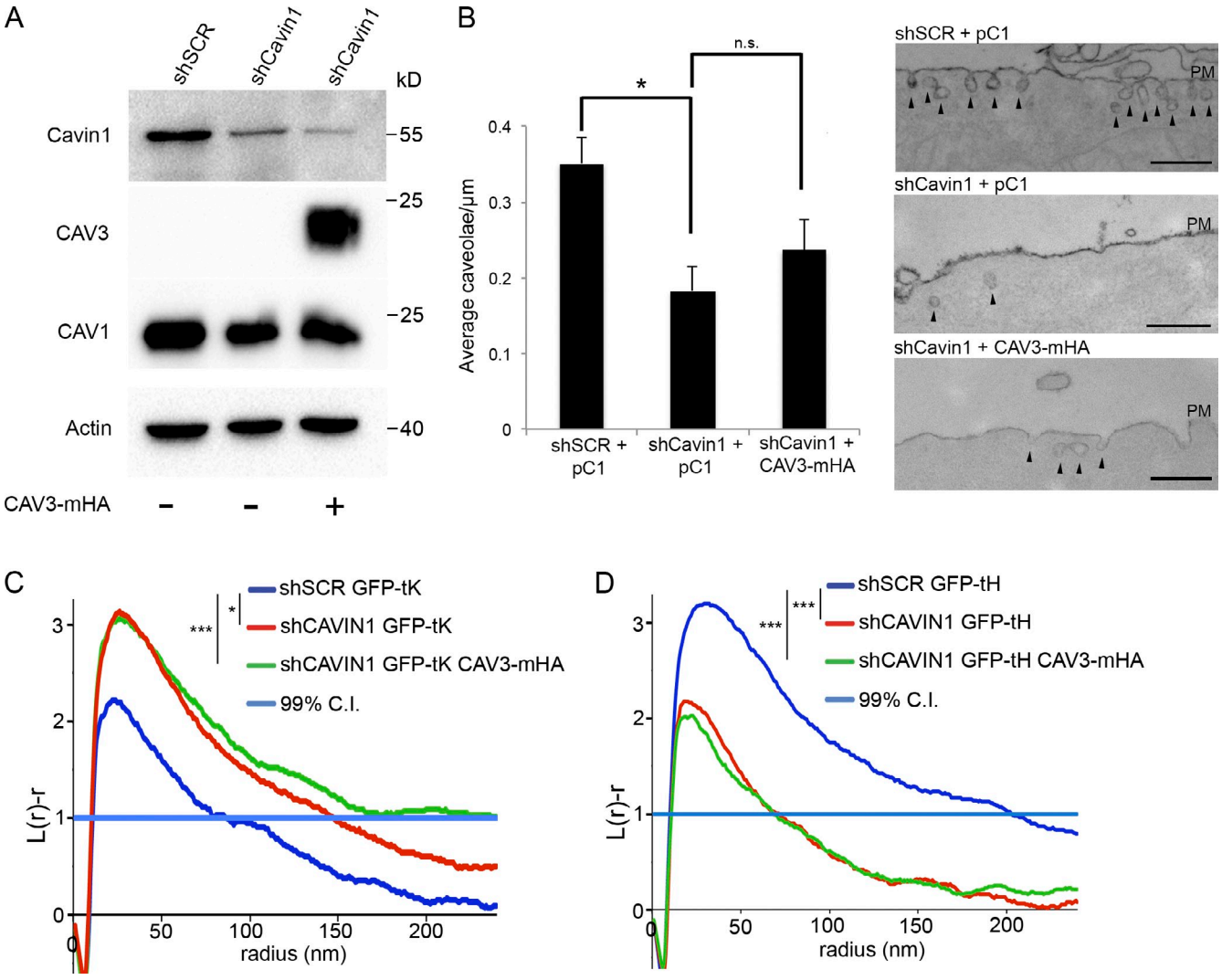

Figure 4. **Down-regulation of Cavin1 reorganizes Ras isoforms similar to CAV1-kd.** (A) Western blot analysis demonstrating significant knockdown of Cavin1 by shRNA-Cavin1 transient transfection. shCavin1 resulted in a slight decrease in CAV1 protein levels; to rescue total caveolin levels back toward control levels, CAV3-mHA was expressed. (B) Loss of Cavin1 resulted in a demonstrable reduction in caveolae at the PM by electron microscopy. (Left) Quantification of caveolae numbers per micrometer of PM from BHK cells (n = 3). (Right) Representative electron micrographs from cells stained with ruthenium red and prepared as described in Materials and methods. Black arrowheads denote caveolae. Bars, 500 nm. Statistical significance was determined by two-tailed Student's t tests. (C) Increased nanoclustering of GFP-tK was observed in Cavin1-kd cells when comparing scrambled control to Cavin1-kd. No rescue was observed upon expression of CAV3-mHA (n = 8, n = 12, and n = 11 for control, shCavin1, and shCavin1 + CAV3-mHA, respectively). (D) Conversely, GFP-tH nanoclustering was reduced by Cavin1 down-regulation. Expression of CAV3-mHA did not return the nanoclustering of shCavin1 back to control levels (n = 12, n = 11, and n = 13 for control, shCavin1, and shCavin1 + CAV3-mHA, respectively). Statistical significance was determined by bootstrap analysis. *, P < 0.05; ***, P < 0.001.

PM cholesterol levels as significant co-clustering was observed between RFP-tH and GFP-H-RasG12V after MβCD treatment (Fig. 3, D and E). No colocalization was observed in untreated control cells nor those administered with αCD (Fig. 3 D). Together the results show that K-Ras nanoclustering is enhanced but H-Ras nanocluster formation is compromised in CAV1-deficient cells.

Caveolae-dependent reorganization of Ras nanoclustering

Previous work has shown that Cavin1 is a critical structural component of caveolae (Hill et al., 2008). Knockdown of Cavin1 was performed to determine if the reorganization of Ras was a result of a specific loss of CAV1 or due to the loss of

expression of CAV3-mHA. (B) Control and CAV1-kd cells expressing GFP-H-RasG12V demonstrated similar nanoclustering levels (n = 15, n = 10, and n = 12 for control, CAV1-kd, and CAV1-kd + CAV3-mHA, respectively). (C) Bivariate analysis of immunogold-labeled spatial point patterns of control and CAV1-kd cells cotransfected with RFP-tH and GFP-H-RasG12V. A significant increase in co-clustering was observed between tH and H-RasG12V in CAV1-kd cells compared with control (n = 13), indicating a disruption to the lateral segregation of H-Ras in the absence of CAV1. (D) Treatment of wild-type BHK cells with MβCD expressing RFP-tH and GFP-H-RasG12V significantly increased the colocalization between tH and H-Ras.GTP (n = 12 for untreated control, n = 14 for MβCD treatment, and n = 15 for αCD treatment). (E) FLIM-FRET analysis confirming an increase in colocalization between tH and H-RasG12V in CAV1-kd BHK cells and a specific reduction in GFP lifetime in control cells after MβCD treatment. Bars, 20 µm. Statistical significance was determined by bootstrap analyses (*, P < 0.05; ***, P < 0.001) for A–D and one-way ANOVA for E.

Downloaded from http://rupress.org/jcb/article-pdf/204/5/777/1583044/jcb_201307055.pdf by guest on 24 April 2024

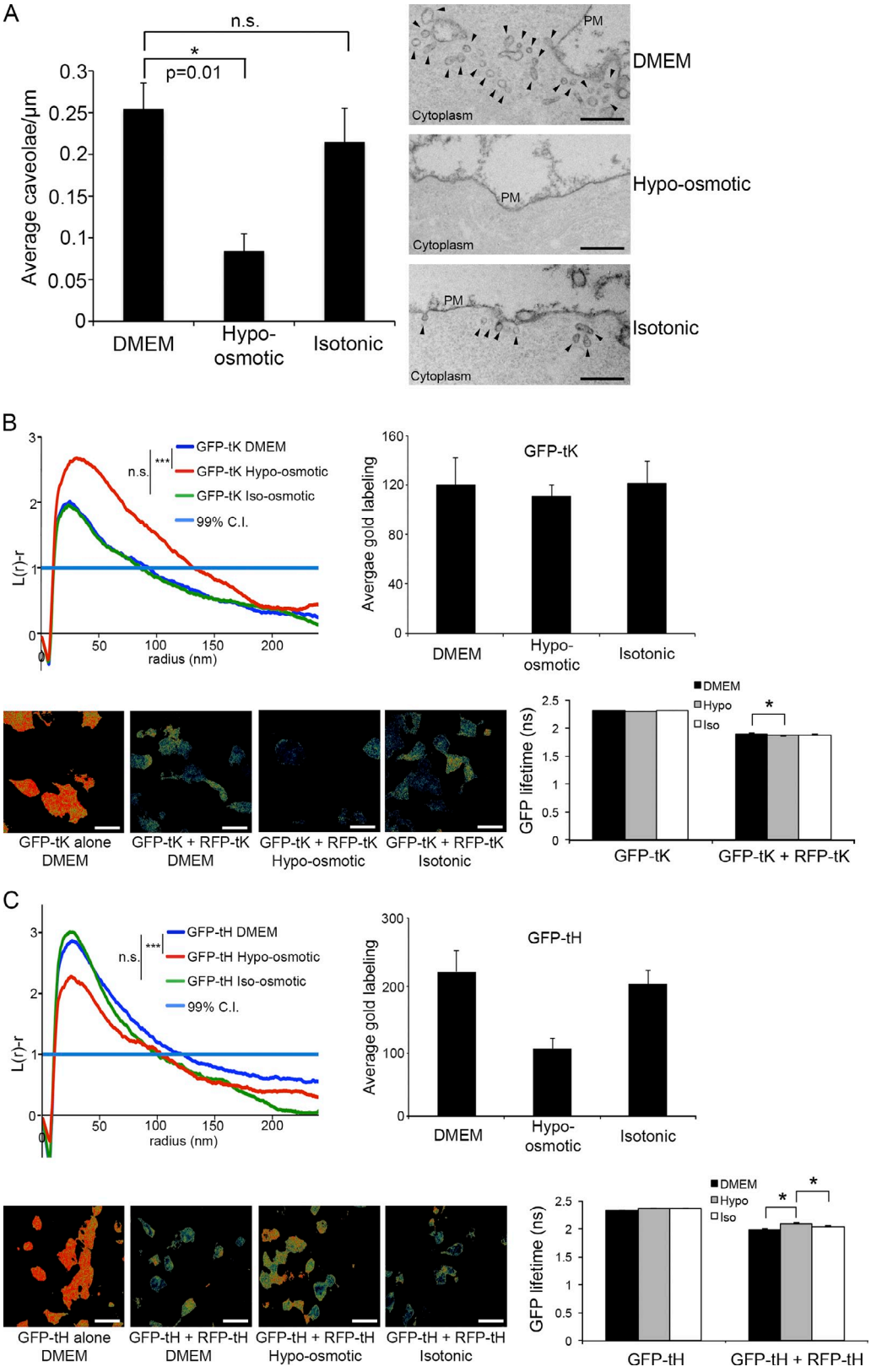

Figure 5. **Loss of caveolae by modulation of cellular osmotic pressure results in similar reorganization of Ras isoforms at the PM.** (A) Wild-type BHK cells were subjected to iso-osmotic, hypo-osmotic, and isotonic conditions and assayed for density of caveolae by electron microscopy. (Left) Quantification of caveolae numbers per micrometer of PM from BHK cells (n = 3). (Right) representative electron micrographs from cells stained with ruthenium red and prepared as described in Materials and methods. Black arrowheads denote caveolae. Bars, 500 nm. (B, top left) Increased nanoclustering of GFP-tK was observed in cells treated with hypo-osmotic medium (n = 13) when compared with DMEM (n = 14). No differences were observed when cells were subjected to isotonic medium (n = 20). (Top right) Quantification of the average amount of labeling per 1 µm^2 of PM lawns in cells transfected with GFP-tK. (Bottom left) FLIM-FRET images of BHK cells expressing tK and treated with different osmotic conditions. Bars, 20 µm. (Bottom right) A significant increase in

Downloaded from http://rupress.org/jcb/article-pdf/204/5/777/1583044/jcb_201307055.pdf by guest on 24 April 2024

caveolae in CAV1-kd cells. A ∼60% reduction in Cavin1 was observed upon shRNA knockdown, correlating with only a 15% reduction in CAV1 (normalized to actin levels; Fig. 4 A) and corresponded to an ∼50% loss of caveolae from the PM by EM (n = 3; Fig. 4 B). Strikingly, similar results were observed between CAV1-kd and Cavin1-kd cells; a loss of Cavin1 resulted in a significant increase in the nanoclustering of GFP-tK (Fig. 4 C) and a significant decrease in the nanoclustering of GFP-tH compared with scrambled control cells (Fig. 4 D). As Cavin1 knockdown slightly reduced CAV1 protein levels, we investigated whether CAV3 expression would rescue the effect of loss of Cavin1; no effect was observed on the nanoclustering of GFP-tK or GFP-tH with expression of CAV3-mHA (Fig. 4, C and D). This suggests that loss of caveolae affects the spatial organization of Ras at the PM.

As a further test of this hypothesis we perturbed caveolae acutely using hypo-osmotic media to mechanically flatten caveolae (Sinha et al., 2011). Three experimental conditions were compared, iso-osmotic (DMEM; 320 mOsm), hypo-osmotic (90% H_2O with 10% DMEM; 32 mOsm), and isotonic (10% DMEM with sorbitol and H_2O). Hypo-osmotic treatment caused ∼66% reduction in caveolar density (Fig. 5 A). Clustering analysis using both Ripley K-function spatial point patterns and FLIM-FRET on live cells after hypo-osmotic treatment demonstrated altered nanoclustering of GFP-tH and GFP-tK in a manner that recapitulated the effect of loss of CAV1 and/or Cavin1—namely, a significant increase in the nanoclustering of GFP-tK (Fig. 5 B) and a reduction in the level of nanoclustering of GFP-tH (Fig. 5 C). Strikingly, CAV1-kd cells did not show the same changes in isoform-specific Ras nanoclustering as judged by FLIM-FRET analysis (Fig. S3 C). These data suggest that loss of caveolae, and not caveolin, per se, alter the distribution of Ras proteins, in an isoform-specific manner, on the inner leaflet of the PM.

Loss of CAV1 has differential effects on H-Ras and K-Ras signaling

The formation of Ras.GTP nanoclusters is essential for signal transmission from the PM. We therefore explored whether signaling through H-Ras and K-Ras was differentially sensitive to the loss of CAV1. $CAV1^{-/-}$ and $CAV1^{+/+}$ MEFs were infected with GFP-H-RasG12V or GFP-K-RasG12V lentiviruses and assayed for MAPK activation 3 d later. MAPK activation by GFP-H-RasG12V was inhibited and MAPK activation by GFP-K-RasG12V was enhanced in $CAV1^{-/-}$ MEFs compared with WT MEFs (Fig. 6 A). To further characterize these alterations in cell signaling, control and CAV1-kd BHK cells were transiently transfected with either GFP-H-RasG12V or GFP-K-RasG12V and assayed for MAPK activation. CAV1-kd cells expressing GFP-H-RasG12V demonstrated significantly lower ppERK levels compared with control cells (Fig. 6, B and C). Conversely, GFP-K-RasG12V activation was enhanced in CAV1-kd cells compared with WT (Fig. 6, B and C). To confirm that these changes in MAPK signaling were a direct result of a loss of CAV1/caveolae, we assayed the activation of ppERK in CAV1-kd BHK cells after expression of CAV3-mHA. In accordance with the above data, we observed a significant reduction in ppERK in CAV3-mHA–rescued K-RasG12V–expressing cells and a concurrent increase in ppERK in CAV3-mHA–rescued H-RasG12V–expressing cells (compared with empty vector control-transfected CAV1-kd cells; Fig. S4, A and B). Thus, we observe concordant changes between enhanced K-Ras.GTP nanoclustering and enhanced K-Ras signal transmission and impaired H-Ras.GTP nanocluster lateral segregation and abrogated H-Ras signal transmission.

Furthermore, to determine if these effects were specifically at the level of Ras or independent of Ras, we assayed the activation of the epidermal growth factor receptor (EGFR) in response to EGF stimulation. No significant differences were observed to the phosphorylation of EGFR between control and CAV1-kd BHK cells (Fig. S4 C).

Acute cholesterol depletion abrogates MAPK activation in WT but not $CAV1^{-/-}$ MEFs

We have previously noted an increase in K-Ras gene expression in $CAV1^{-/-}$ mice (Fernández-Rojo et al., 2013); thus, we assayed K-Ras protein levels in $CAV1^{-/-}$ MEFs. Expression was significantly higher compared with WT MEFs (Fig. 7 A), suggesting that Ras signaling in $CAV1^{-/-}$ MEFs may be largely driven by K-Ras as both the protein level is elevated and nanoclustering is enhanced in cells with abrogated CAV1 levels. We have shown previously that K-Ras signal transmission is unaffected by cholesterol depletion, whereas signaling by other Ras isoforms is cholesterol sensitive (Roy et al., 1999, 2005; Prior et al., 2001). Therefore, we compared $CAV1^{+/+}$ and $CAV1^{-/-}$ MEFs for activation of the MAP kinase pathway in response to serum stimulation under normal and cholesterol-depleted conditions. Cells were cultured overnight in the absence of serum and stimulated with 10% fetal calf serum. The kinetics and extent of activation of MEK, ERK, and Akt were similar between $CAV1^{+/+}$ and $CAV1^{-/-}$ MEFs (Fig. 7, B and C). Treatment of $CAV1^{+/+}$ MEFs with MβCD abrogated serum-stimulated activation of MEK, ERK, and Akt. In contrast, serum-induced phosphorylation of MEK and ERK in the $CAV1^{-/-}$ MEFs was unaffected by MβCD and Akt was partially reduced (Fig. 7, B and C). Consistent with previous studies (Frank et al., 2006), cholesterol levels, before and after MβCD treatment, were equivalent

the nanoclustering of tK was observed under hypo-osmotic conditions, indicated by a significant reduction in GFP lifetime (P = 0.04). (C, top left) Decreased nanoclustering of GFP-tH was observed in cells treated with hypo-osmotic medium (n = 11) when compared with DMEM (n = 14). No change to the levels of nanoclustering was observed in cells treated with isotonic medium (n = 14). (Top right) Quantification of the average amount of labeling per 1 μm^2 of PM lawns in cells transfected with GFP-tH. Although a reduction in the total GFP-tH labeling at the PM was observed, these changes in nanoclustering were independent of this decrease, as selection of equivalently labeled spatial point patterns (comparing DMEM to control) demonstrated similar deviations in nanoclustering (Fig. S3, A and B). (Bottom left) FLIM-FRET images of tH-expressing BHK cells under various osmotic conditions. Bars, 20 µm. (Bottom right) A significant increase in GFP lifetime was observed in tH-expressing hypo-osmotic–treated BHK cells, indicating a reduction in nanoclustering. Statistical significance was determined by two-tailed Student's t tests in A, bootstrap analyses in the top left panels of B and C, and one-way ANOVA in the bottom right panels of B and C. *, P < 0.05; ***, P < 0.001.

Downloaded from http://rupress.org/jcb/article-pdf/204/5/777/1583044/jcb_201307055.pdf by guest on 24 April 2024

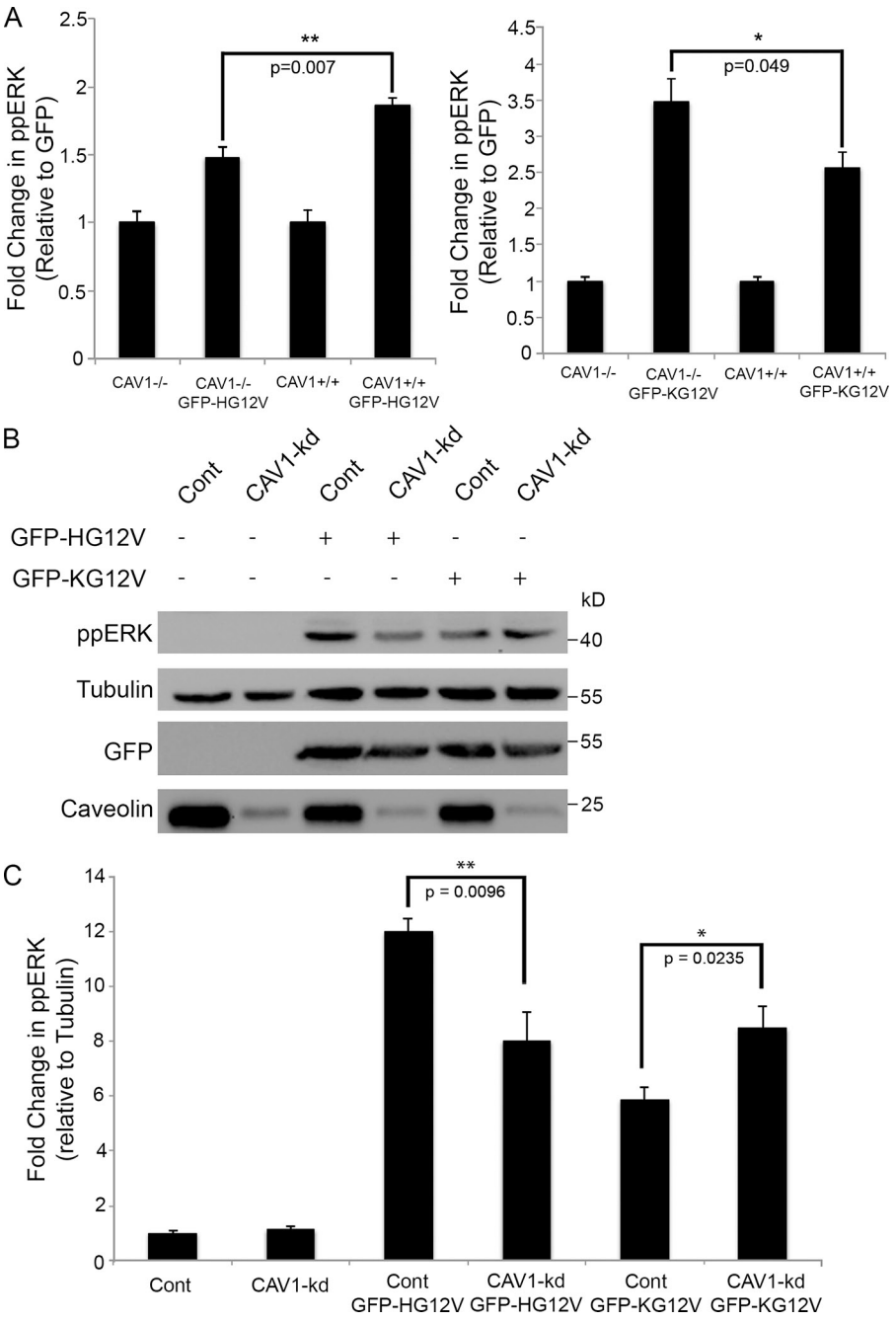

Figure 6. **Differential sensitivity of H-Ras and K-Ras signaling to caveolin loss.** (A) Quantification of Western blots of CAV1$^{-/-}$ MEFs showing enhanced ERK phosphorylation from lentivirus-mediated expression of GFP-K-RasG12V (compared with WT expressing K-RasG12V, P = 0.049) but reduced signal output from H-RasG12V (compared with WT expressing H-RasG12V, P = 0.0069; *n* = 4). Quantification was normalized to GFP levels and performed as described in Abankwa et al. (2008). Statistical significance was determined by two-tailed Student's *t* tests. (B) Western blot analysis of BHK cells transfected with activated Ras isoforms, GFP-H-RasG12V and GFP-K-RasG12V, showing differential and opposing activation of the MAP kinase pathway in response to the expression of each construct (*n* = 4). (C) Quantification indicates that a loss of CAV1 results in a significant reduction in MAP kinase signaling through H-Ras and a concurrent increase in K-Ras–mediated MAP kinase signaling (independently compared with scrambled controls). Statistical significance was determined by two-tailed Student's *t* test analyses.

between CAV1$^{+/+}$ and CAV1$^{-/-}$ cells (Fig. 7 D). Adenoviral re-expression of CAV1 into CAV1$^{-/-}$ MEFs rescued sensitivity to cholesterol depletion (Fig. 8, A and B). Similarly, acute cholesterol depletion with MβCD inhibited EGF-stimulated MAPK activation in control BHK cells but not CAV1-kd cells (Fig. S5). Thus, loss of CAV1 expression renders agonist-stimulated MAPK activation insensitive to cholesterol depletion, an effect that is likely mediated by a switch to K-Ras signaling.

Discussion

Caveolins, crucial structural proteins of caveolae, have been widely proposed to maintain signaling proteins in inactive conformations through direct protein–protein interactions, a hypothesis that now seems unlikely (Collins et al., 2012). A role, however, for caveolae as more general regulators of PM structure and function has received less attention. Through the use of a range of techniques, including EM, signaling assays, lipidomics, FLIM-FRET, and gene expression analysis we now show that loss or reduced levels of CAV1/Cavin1/caveolae have profound implications for PM organization. These effects include a major shift in the cellular lipid profile, a change in sensitivity to cholesterol perturbation, increased clustering of PS, and significant changes to the operation of Ras signaling pathways.

The most significantly deregulated cellular pathways in CAV1$^{-/-}$ MEFs were involved in glycosphingolipid (GSL) and sphingolipid (SL) metabolism. Key genes affected included *ST3Gal5* (*Siat9 or GM3 synthase*) and *Ppap2A* (Lpp1), changes

Downloaded from http://rupress.org/jcb/article-pdf/204/5/777/1583044/jcb_201307055.pdf by guest on 24 April 2024

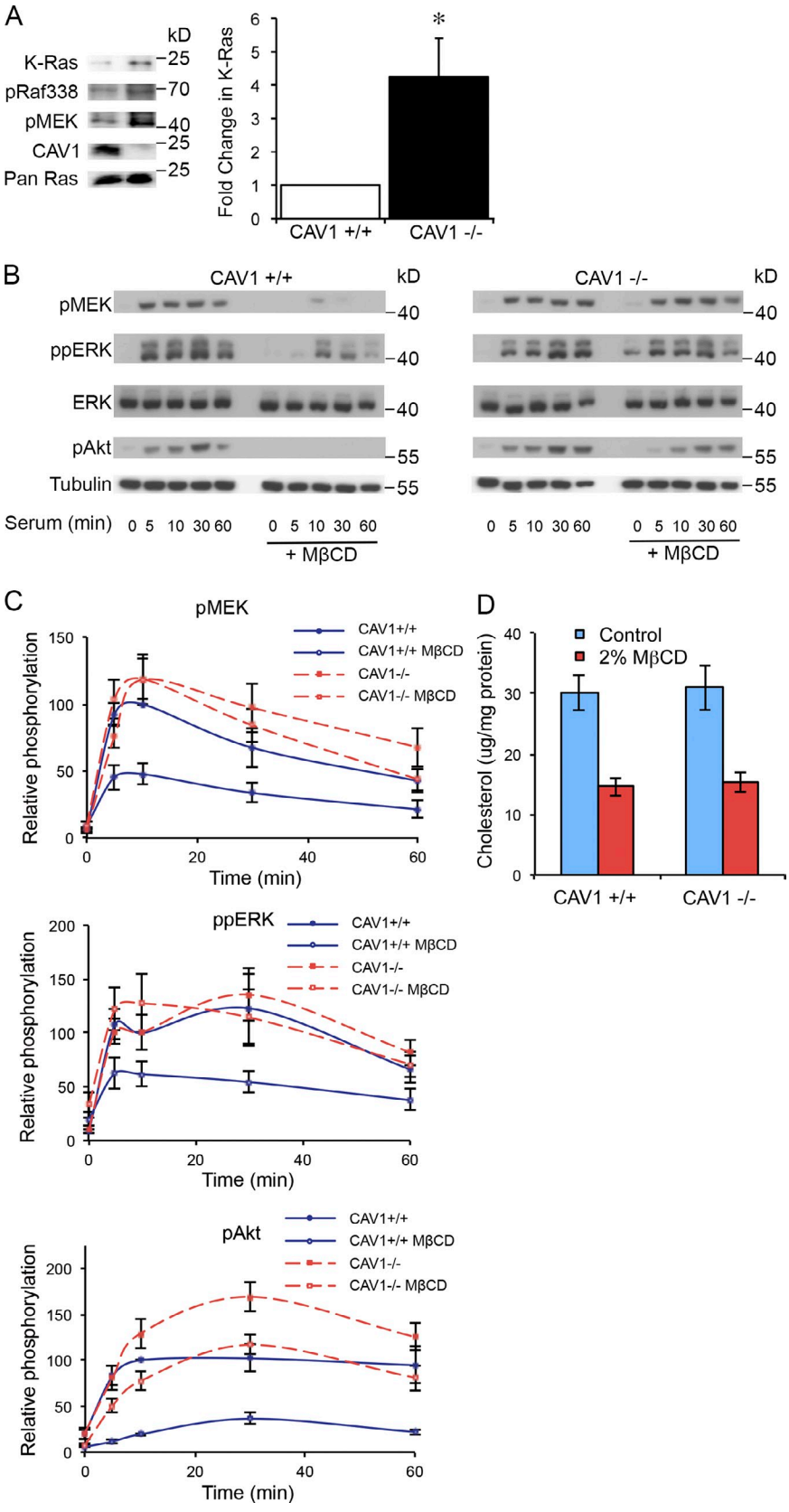

Figure 7. **Cholesterol depletion in MEFs causes loss of MAP kinase activation in WT but not CAV1$^{-/-}$ cells.** (A) Western blot analysis of K-Ras in MEFs demonstrates an approximately four-fold increase in protein level that translates into downstream up-regulation of MAPK signaling in CAV1$^{-/-}$ cells. Statistical significance was determined by two-tailed Student's *t* test analysis. *, $P < 0.05$ ($n = 3$). (B) MEFs were serum starved overnight, treated with 2% MβCD for 30 min, and stimulated with 10% FCS for various times. CAV1$^{+/+}$ and CAV1$^{-/-}$ MEFs respond to serum stimulation in a similar manner. Cholesterol depletion before serum stimulation inhibited phosphorylation of pMEK, ppERK, and pAkt in CAV1$^{+/+}$ MEFs but not in CAV1$^{-/-}$ MEFs ($n = 3$). (C) Activation profiles of CAV1$^{+/+}$ and CAV1$^{-/-}$ MEFs after serum stimulation with or without cholesterol depletion. (D) Cholesterol levels are equivalent between untreated and cholesterol-depleted CAV1$^{+/+}$ and CAV1$^{-/-}$ cells ($n = 3$).

that were cell autonomous and recapitulated in knockdown cells. These changes correlated with widespread alterations to the cellular lipid profile including a significant decrease in total GM3 content and significant alterations in specific, but not total, cellular GM3 precursor levels. Strengthening the links between GM3 and CAV1, comparative lipidomic studies have shown that GM3 is enriched in caveolae (Ortegren et al., 2004), and expression of GM3 synthase (SAT-1) up-regulates of CAV1

Downloaded from http://rupress.org/jcb/article-pdf/204/5/777/1583044/jcb_201307055.pdf by guest on 24 April 2024

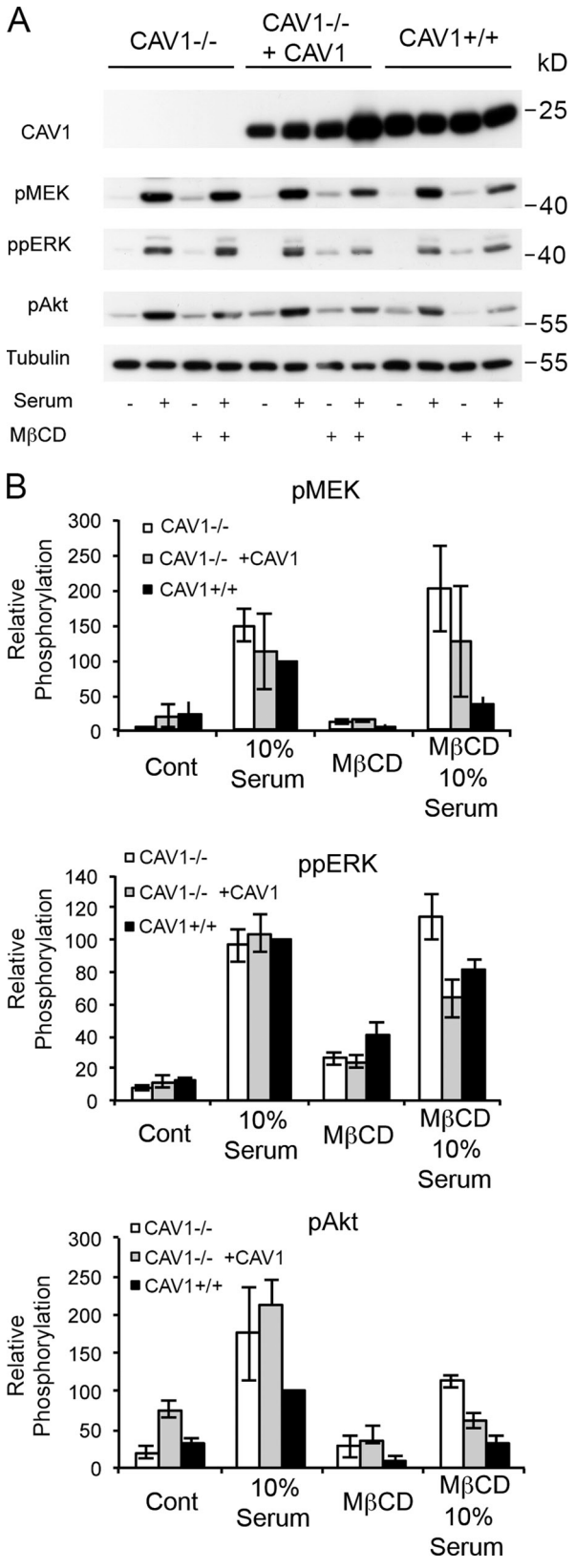

Figure 8. **Re-expression of CAV1 rescues sensitivity to cholesterol depletion in CAV1$^{-/-}$ MEFs.** (A) Adenoviral expression of CAV1 in CAV1$^{-/-}$ MEFs rescues the sensitivity of the MAPK pathway signaling to cholesterol depletion. (B) Quantification of ppERK, pMEK, and pAkt levels in CAV1$^{+/+}$, CAV1$^{-/-}$, and CAV1$^{-/-}$ expressing CAV1 MEFs (n = 3).

expression (Prinetti et al., 2010). This is consistent with the reciprocal result observed here; CAV1 deficiency reduces GM3 levels. Experiments in Siat9$^{-/-}$ (GM3 synthase knock-out) MEFs demonstrated a reduction in GM3 directly correlated with increased cell motility and an up-regulation of the Ras/Raf/MAP kinase pathway (Hashiramoto et al., 2006). Although it has been shown that different phospholipids differentially affect H-Ras and K-Ras (Kuroda et al., 1996), GM3 has been postulated as a key regulator for cellular signaling pathways, including those mediated by Ras proteins (Garofalo et al., 2002). Although the lipidomics performed in this study comprised a whole-cell analysis of differentially affected lipid species comparing CAV1$^{+/+}$ to CAV1$^{-/-}$ MEFs and not specific isolations of PMs from these two cell types, it is necessary to consider the dynamics of PM turnover. Previous work has indicated a turnover rate for the whole PM at ∼20 min (Hao and Maxfield, 2000). This suggests that any proportional whole-cell change in specific lipid species will likely be reflected in proportional changes to all membranes in a closed dynamic system. Regardless, it is increasingly apparent that the function of the PM requires hundreds of different lipids, not to simply function as a solvent in which membrane proteins are dissolved, but to allow formation of distinct dynamic assemblies required for specific signaling events, to maintain and adjust the fluidity of the PM for spatial control, and to regulate numerous other crucial cellular processes. The global changes in cellular lipids described here presumably reflect the need to maintain the functional organization of the cell surface despite the loss of caveolae.

The assembly of Ras nanoclusters involves interactions between membrane-binding elements on Ras, specific lipids of the PM, an intact actin cytoskeleton, and the recruitment of cytosolic protein scaffolds (Prior et al., 2003a; Rotblat et al., 2004; Plowman et al., 2005; Gorfe et al., 2007; Belanis et al., 2008). Perturbations of the lipid content would be expected to influence Ras nanocluster assembly. Furthermore, because each Ras isoform has a different lipid anchor and different hyper-variable flanking region that participates in membrane interactions (Hancock, 2003), the consequence of changes to PM lipid composition would be expected to differentially affect nanoclustering by different Ras isoforms. We therefore propose that the changes in cellular lipid composition and in PM lipid organization that follow from caveolae/CAV1 loss are directly responsible for the profound changes in Ras nanoclustering that we report here. Using both immunoEM and FLIM-FRET methods, and despite the inherent differences in respective resolutions of these techniques (∼10 nm for immunoEM and ∼50 nm for FLIM-FRET), we consistently observed an increase in K-Ras nanoclustering upon loss of caveolae/CAV1 and an increase in clustering of PS. The PS content of the inner leaflet contributes significantly to the electronegative ζ-potential that provides membrane affinity for polybasic domain-anchored proteins such as K-Ras. Depleting the inner leaflet of PS reduces the total amount of K-Ras localized to the PM and also impairs K-Ras nanoclustering (Cho et al., 2012). There are many links between PM PS and caveolar function that raise the possibility that PS is a key element in caveolar formation (Parton and del Pozo, 2013). Enrichment of PS on the cytoplasmic face of caveolae has been reported (Fairn

Downloaded from http://rupress.org/jcb/article-pdf/204/5/777/1583044/jcb_201307055.pdf by guest on 24 April 2024

et al., 2011), all four mammalian cavin proteins bind PS in vitro, and caveolin peptides modulate PS distribution in model systems (Wanaski et al., 2003). Reciprocally, we now show that caveolae directly or indirectly influence noncaveolar pools of PS providing an explanation for increased clustering and activity of K-Ras. Because CAV1-depleted cells have increased cortical actin (Grande-García et al., 2007), this may also cooperate with changes in PS distribution to facilitate K-Ras nanoclustering. Changes to H-Ras spatial organization in CAV1-depleted cells were more complex. Clustering of GFP-tH and H-Ras.GDP, which form cholesterol-dependent nanoclusters, was inhibited; H-Ras.GTP nanoclusters formed but the composition was aberrant because they contained significant amounts of H-Ras.GDP. This spatial phenotype reflects a failure of efficient lateral segregation where activation state of the G-domain reorganizes the interactions of the C-terminal anchor with the lipid bilayer to drive H-Ras.GDP and H-Ras.GTP into different, spatially nonoverlapping nanoclusters (Abankwa et al., 2007, 2008; Gorfe et al., 2007). We now show here that CAV1 depletion, which destabilizes H-Ras.GDP L_o domains, also promotes formation of mixed heterotypic clusters of H-Ras.GTP and H-Ras.GDP, which as in NSAID-treated cells (Zhou et al., 2012) are compromised for signal transmission. Previous work has demonstrated the essential role of nanoscale clustering of H- and K-Ras for signaling function (Tian et al., 2007). The positive and negative changes to K- and H-Ras clustering in cells with decreased CAV1 therefore fully explain the concomitant enhanced MAPK activation by K-RasG12V (K-Ras.GTP) and impaired MAPK activation by H-RasG12V. In non-Ras transformed CAV1-depleted cells these reciprocal changes in endogenous H-Ras and K-Ras activity result in a largely unchanged growth factor–stimulated MAP kinase activation profile. However, the EGF-MAPK signaling is rendered insensitive to cholesterol depletion, as shown both in MEFs lacking CAV1 and BHK cells with reduced CAV1. The change in cholesterol sensitivity did not reflect alterations in the level of cholesterol depletion but is an interesting consequence of a shift to K-Ras–mediated signaling. The requirement for increased activity of the K-Ras pathway is also perhaps reflected in the up-regulation of K-Ras at the protein level in CAV1$^{-/-}$ cells.

We have previously proposed that caveolae could act as a regulated store for specific lipids, which are highly concentrated in caveolae (Parton and Simons, 2007). Cells lacking caveolae would lose this regulatory control over PM lipids. The change in lipid composition might explain the reported decrease in membrane order in CAV1$^{-/-}$ cells (Gaus et al., 2006). Furthermore, the loss of caveolae from the PM and change in membrane order as cells lose contact with the substratum (Grande-García et al., 2007) may represent an acute manifestation of the loss of caveolae shown here. This hypothesis is given greater weight with our observation that hypo-osmotic treatment, resulting in a rapid disassembly of caveolae, was causal in generating a similar nanoscale PM reorganization of H- and K-Ras as those generated by down-regulation of caveolar structural elements. These data, when combined with recent work showing shear stress induces dramatic and fast reduction in membrane order in endothelial cells (Yamamoto and Ando, 2013), lend themselves to a hypothesis whereby an individual caveola may function as an organizational unit that can flatten into the PM and release specific lipids that modulate the local lipid environment to respond to changes in cellular stress. Cross talk between mechanosensitive caveolae and cellular lipids strengthens the proposed functional similarity to eisosomes in yeast in which eisosome mechanosensation is translated into alterations in glycosphingolipid metabolism as a protective mechanism (Berchtold et al., 2012; Parton and del Pozo, 2013). We suggest that the loss of CAV1/caveolae from the PM has wide-reaching and dramatic effects on PM dynamics due to these lipid changes. This results in loss of specific lipid-based organization of signaling proteins and their function. In view of the dramatic effects on Ras isoform organization and activity described here, we speculate that caveolae play a crucial and dynamic role in the lipid-based regulation of other key signaling pathways, and this mechanism underlies the widespread effects of caveolin loss on specific signaling events. In addition, these results demonstrate that mechanical alterations causing caveolar disassembly can be transduced into lipid changes in the PM with resulting changes in signal transduction pathways, linking caveolar mechanosensing with lipid regulation.

Materials and methods

Cell culture, transfections, and lentiviral-mediated down-regulation of CAV1

MEFs were cultured in DMEM substituted with 10% fetal calf serum (FCS). BHK cells were cultured in DMEM substituted with 10% heat-inactivated serum supreme (HISS) and transfected with Lipofectamine 2000 (Invitrogen) as per the manufacturer's instruction. Stable CAV1 knockdown BHK cell lines were developed using SHVRS MISSION shRNA lentiviral particles (Mission shRNA set; Sigma-Aldrich) against mouse caveolin-1 following the manufacturer's protocols. Cells were selected using 1 µg/ml puromycin and pooled populations were used for experiments. CAV1 protein levels were determined by Western blot analysis using α-CAV polyclonal antibody (BD).

Western blotting

WT and CAV1$^{-/-}$ MEFs were serum starved overnight before stimulation with 10% FCS for variable times (0–60 min). BHK cells were serum starved for 3 h before treatment with 1% methyl-β-cyclodextrin for 1 h. Varying concentrations (0–20 ng/ml) of EGF in serum-free DMEM was used to stimulate the MAPK pathway for 10 min. Cells were washed three times in cold phosphate-buffered saline (PBS) and whole-cell lysates were produced (50 mM Tris, pH 7.5, 75 mM NaCl, 1% Nonidet P-40, plus protease inhibitors and phosphatase inhibitors [Roche]). 20 µg of protein was run on sodium dodecyl sulfate-PAGE (SDS-PAGE; 12% acrylamide) and immunoblotted with α-ppERK antibody (Cell Signaling Technology), α-caveolin (BD), α-GFP (Roche), α-tubulin (Sigma-Aldrich), and α-cavin1 (Sigma-Aldrich). Band intensities were quantified using ImageJ (National Institutes of Health, Bethesda, MD).

Immunogold labeling of plasma membrane sheets and statistics

Immunogold labeling was performed exactly as described previously (Prior et al., 2003a,b; Plowman et al., 2005, 2008). In brief, PM lawns were generated, fixed (4% paraformaldehyde and 0.1% glutaraldehyde in KOAc buffer [25 mM Hepes, 115 mM KOAc, 2.5 mM $MgCl_2$ at pH 7.4]) and immunolabeled with 5 nm directly conjugated α-GFP antibody (rabbit). Imaging of PM lawns was performed on an electron microscope (model 1011; JEOL) at 100,000×, fitted with a 4K × 4K soft imaging camera (Morada; Olympus) with twofold binning. 1-µm^2 areas of PM lawn were selected and the position of each immunogold was digitized into a set of *x* and *y* coordinates using ImageJ. Univariate and bivariate spatial point pattern analyses were performed as described previously (Prior et al., 2003a; Plowman et al., 2005, 2008) and the statistical significance of differences between replicated point patterns was evaluated in bootstrap tests constructed as described previously (Diggle et al., 2000; Plowman et al., 2005). The univariate L(r)-r curve is a graphical plot of the extent of

Downloaded from http://rupress.org/jcb/article-pdf/204/5/777/1583044/jcb_201307055.pdf by guest on 24 April 2024

cluster formation over a given radius, where the vertical axis represents the extent of clustering (L(r)-r values greater than 1 are said to be clustered, values between 1 and −1 are said to be in a state of complete spatial randomness, and values less than −1 are said to be spatially dispersed) and the horizontal axis represents the radius of the nanocluster. The bivariate $L_{biv}(r)$-r curve is a graphical representation of the extent of co-clustering between different populations of spatial point patterns over a given radius ($L_{biv}(r)$-r values greater than 1 are indicative of two populations of spatial point patterns that co-cluster together, whereas values between 1 and −1 are indicative of two populations of spatial point patterns arranged in a state of spatial randomness with respect to one another).

FLIM combined with FRET (FLIM-FRET)

FRET measurements based on fluorescence lifetime are advantageous over intensity-based FRET measurements because fluorescence lifetime is an inherent property of the fluorophore and is independent of excitation source, detection gain, optical loss, and variation in fluorophore concentrations. Fluorescence lifetime is also significantly less sensitive to donor/acceptor ratio (Zhou et al., 2010, 2012). In brief, ∼200,000 control or CAV1-kd BHK cells were seeded on glass coverslips placed in 6-well plates overnight before transient transfection with either construct of GFP-tagged protein and empty vector (pC1) or constructs of GFP-tagged and RFP-tagged proteins. Cell fixation with 4% PFA and quenching with 50 mM NH_4OH were performed ∼18 h after transfection. GFP in fixed cells was excited by a 3-W 497-nm sinusoidally simulated modulating light-emitting diode (LED) mounted on a FLIM unit (Lambert Instruments) attached a wide-field microscope (Eclipse; Nikon). GFP excitation was achieved using a sinusoidally simulated modulating 3-W 497-nm LED at 40 MHz under epi-illumination via a 60× Plan-Apo/1.4 NA oil emersion lens, and images were acquired for ∼300 ms. Three individual experiments were conducted for each condition. The whole-cell GFP lifetime values from at least 60 cells were imaged, pooled, and averaged, and statistical analysis was performed using one-way ANOVA and presented as mean ± SEM.

Electron microscopy and quantification of caveolae

Fixation, embedding, and sectioning were performed as follows. BHK cells were fixed with 2.5% glutaraldehyde containing 1 mg/ml of ruthenium red in 0.1 M cacodylate buffer (pH 7.4). Cells were post-fixed with 1% osmium tetroxide with 1 mg/ml of ruthenium red for 1 h at room temperature and serially dehydrated with ethanol. Cells were embedded in increasing ratios of LX-112 resin/ethanol to 100% resin, and polymerized overnight at 60°C. Vertical ultrathin (60 nm) sections were cut on a microtome (model UC6; Leica) and imaged on an electron microscope (model1011; JEOL) at 80 kV. Quantifications were performed as follows: the perimeters of ∼20 cells (per experimental condition) were measured and the number of caveolae from each cell was quantified and averaged across all 20. The average number of caveolae per µm of PM was generated from three separate repeats of the same experimental conditions.

Animals and mouse embryonic fibroblasts

$CAV1^{+/+}$ and $CAV1^{-/-}$ mice and MEF isolation and culture were described in Fernández et al. (2006). In brief, $CAV1^{-/-}$ mice were generated by genetic excision of the third exon of the CAV1 gene that encodes the intramembrane domain, CAV1 palmitoylation sites, and the scaffolding domain. For the isolation of MEFs, mice were kept under a controlled humidity and lighting schedule with a 12-h dark period. All animals received care in compliance with institutional guidelines regulated by the Australian government. Primary MEFs were obtained from day 13.5 embryos, which were decapitated, thoroughly minced, and trypsinized in 1 ml of 0.05% trypsin and 0.53 mM EDTA (Life Technologies) for 20 min at 37°C. 10 ml of complete medium (DMEM) supplemented with 10% FBS, 2 mM glutamine, 100 U/ml penicillin, and 100 µg/ml streptomycin (Life Technologies) was used to inactivate the trypsin and resuspend the dissociated cells. Cells were plated on a 10-cm plate and cultured in a 37°C, 5% CO_2 incubator.

CAV1 knockdown in AML12 hepatocytes

Transient CAV1 knockdown in AML12 hepatocytes using specific siRNA was performed as described for MEFs in Fernández et al. (2006).

Quantitative real-time PCR and primers

RNA was extracted using RNAeasy (QIAGEN), and 4–5 µg was reverse transcribed. Quantitative RT-PCR was performed in triplicate on 6–9 independent RNA preparations. cDNA levels were analyzed in PCR reactions with SYBR green (Applied Biosystems), and the relative level of expression was normalized using 18S ribosomal RNA. Statistical analysis was performed on the average of 3–6 independent assays using Student's *t* test. Primer sequences can be provided on request.

Lipidomic analysis and lipid extraction

Lipids were extracted using a modified Bligh and Dyer protocol (Bligh and Dyer, 1959). The whole procedure was performed on ice and reagents were pre-chilled on ice before lipid extraction. In brief, cells (10-cm dish) were scraped in 400 µl methanol, collected, and 200 µl chloroform was added to obtain a chloroform/methanol ratio of 1:2. Samples were thoroughly vortexed three times for 1 min and incubated on ice for another 4 min. Subsequently, 300 µl of chloroform and 200 µl of 1 M KCl were added, samples were vortexed three times for 30 s, and incubated on ice for 1 min. Finally, phases were separated by centrifuging samples for 2 min at 9,000 rpm in a pre-chilled bench-top microcentrifuge. The organic phase was collected, transferred to a clean microcentrifuge tube, dried in a speed vacuum, and stored at −80°C.

Mass spectrometry analysis of lipid species

Mass spectrometry analysis was slightly modified from Chan et al. (2008). For quantitative analysis of glycerophospholipids and sphingolipids a high performance liquid chromatography (HPLC) mass spectrometry (MS) was used. Multiple reaction monitoring (MRM) measurements were performed on a triple quadrupole instrument (ABI 3200QT; Applied Biosystems) directly connected to the LC. The HPLC method was adapted from Pettitt et al. (2001). All samples were dissolved in chloroform/methanol (1:1, vol/vol) and spiked with a mixture of internal standards for each lipid class: dimyristoyl-glycero-phosphoserine (DMPS); 1,2-dimyristoyl-glycero-3-phosphoethanolamine (DMPE); 1,2-dimyristoyl-glycero-3-phosphocholine (DMPC); 1,2-dioctanoyl-glycero-3-phosphoinositol (C8PI); lauroyl sphingomyelin (L-SM); *N*-heptadecanoyl-D-erythro-sphingosine (C17 ceramide); and D-glucosyl-β1-1′-*N*-octanoyl- D-erythro-sphingosine (C8 glucosyl ceramide (1:1:1:1:1:0.5:0.5, vol/vol; Avanti Polar Lipids, Inc.) were used to measure glycerophosphatidylserine, glycerophosphatidylethanolamine and plasmalogen-PE (pl-PE), glycerophosphatidylcholine and ePC, glycerophosphoinositols, sphingomyelin, and ceramide (Cer) and monohexosyl ceramide (MonoHexCer), respectively. PS, PE, PI, and GM3 were measured in the negative ion mode whereas PC, SM, Cer, and MonoHexCer were analyzed in the positive ion mode. Signal intensities for each lipid species were extracted based on their retention time (PS, 5 min; PE, 1 min; PC, 10 min; PI, 5 min; GM3, 5 min; SM, 10 min; Cer, 0.3 min; and MonoHexCer, 4.5 min) and were converted to their level (moles) in each sample by normalization to the appropriate internal standard. GM3 levels were normalized using the PI internal standard. The final lipid molar fractions (the amount of each lipid was measured in moles and then converted to a fraction of the total) of each sample were obtained by cross-normalizing the lipid level of each fraction measured (Chan et al., 2008) and a log-fold (KO/WT) ratio was calculated to present data in a heat plot.

Online supplemental material

Fig. S1 demonstrates that a loss of CAV1 results in dramatic changes to the abundance of a variety of different glycosphingolipid species and phospholipid species in MEFs. Fig. S2 shows the consistent nature of loss of CAV1 on the nanoclustering of the different Ras isoforms, namely GFP-K-Ras (WT) nanoclustering is increased in CAV1-kd cells and GFP-H-Ras (WT) nanoclustering is decreased. Fig. S3 demonstrates that the loss of labeling observed when GFP-tH–expressing cells are subjected to hypo-osmotic treatment is independent of the changes in nanoclustering and that CAV1-kd cells do not respond in a similar manner to hypo-osmotic treatment when compared with control cells. Fig. S4 shows rescue of CAV1-kd cells expressing either activated H-Ras or K-Ras with CAV3 expression restores MAPK signaling toward control cell levels. Fig. S5 demonstrates that CAV1-kd BHK cells are similarly insensitive to cholesterol depletion–mediated abrogation of the MAPK pathway analogous to $CAV1^{-/-}$ MEFs. Online supplemental material is available at http://www.jcb.org/cgi/content/full/jcb.201307055/DC1. Additional data are available in the JCB DataViewer at http://dx.doi.org/10.1083/jcb.201307055.dv.

The authors acknowledge the facilities and the scientific and technical assistance of the Australian Microscopy and Microanalysis Research Facility (AMMRF) at the Centre for Microscopy and Microanalysis, the University of Queensland (Queensland, Australia). The authors also acknowledge the Australian Cancer Research Facility (ACRF)/IMB Dynamic Imaging Facility for Cancer Biology, established with funding from the ACRF.

This work was supported by the National Health and Medical Research Council of Australia, through grants and research fellowships to R.G. Parton (511055, 569542, 1045092, and 1037320) and by grant GM066717

Downloaded from http://rupress.org/jcb/article-pdf/204/5/777/1583044/jcb_201307055.pdf by guest on 24 April 2024

from the National Institutes of Health, General Medical Sciences (J.F. Hancock). M.A. Fernández-Rojo was supported by the Program of MEC/Fulbright postdoctoral fellowships from the Spanish Government and by the Diabetes Australia Research Trust (DART).

The authors declare no competing financial interests.

Submitted: 9 July 2013
Accepted: 15 January 2014

References

Abankwa, D., A.A. Gorfe, and J.F. Hancock. 2007. Ras nanoclusters: molecular structure and assembly. *Semin. Cell Dev. Biol.* 18:599–607. http://dx.doi.org/10.1016/j.semcdb.2007.08.003

Abankwa, D., A.A. Gorfe, and J.F. Hancock. 2008. Mechanisms of Ras membrane organization and signalling: Ras on a rocker. *Cell Cycle*. 7:2667–2673. http://dx.doi.org/10.4161/cc.7.17.6596

Belanis, L., S.J. Plowman, B. Rotblat, J.F. Hancock, and Y. Kloog. 2008. Galectin-1 is a novel structural component and a major regulator of h-ras nanoclusters. *Mol. Biol. Cell*. 19:1404–1414. http://dx.doi.org/10.1091/mbc.E07-10-1053

Berchtold, D., M. Piccolis, N. Chiaruttini, I. Riezman, H. Riezman, A. Roux, T.C. Walther, and R. Loewith. 2012. Plasma membrane stress induces relocalization of Slm proteins and activation of TORC2 to promote sphingolipid synthesis. *Nat. Cell Biol.* 14:542–547. http://dx.doi.org/10.1038/ncb2480

Bligh, E.G., and W.J. Dyer. 1959. A rapid method of total lipid extraction and purification. *Can. J. Biochem. Physiol.* 37:911–917. http://dx.doi.org/10.1139/o59-099

Carozzi, A.J., S. Roy, I.C. Morrow, A. Pol, B. Wyse, J. Clyde-Smith, I.A. Prior, S.J. Nixon, J.F. Hancock, and R.G. Parton. 2002. Inhibition of lipid raft-dependent signaling by a dystrophy-associated mutant of caveolin-3. *J. Biol. Chem.* 277:17944–17949. http://dx.doi.org/10.1074/jbc.M110879200

Chan, R., P.D. Uchil, J. Jin, G. Shui, D.E. Ott, W. Mothes, and M.R. Wenk. 2008. Retroviruses human immunodeficiency virus and murine leukemia virus are enriched in phosphoinositides. *J. Virol.* 82:11228–11238. http://dx.doi.org/10.1128/JVI.00981-08

Cho, K.J., J.H. Park, A.M. Piggott, A.A. Salim, A.A. Gorfe, R.G. Parton, R.J. Capon, E. Lacey, and J.F. Hancock. 2012. Staurosporines disrupt phosphatidylserine trafficking and mislocalize Ras proteins. *J. Biol. Chem.* 287:43573–43584. http://dx.doi.org/10.1074/jbc.M112.424457

Collins, B.M., M.J. Davis, J.F. Hancock, and R.G. Parton. 2012. Structure-based reassessment of the caveolin signaling model: do caveolae regulate signaling through caveolin-protein interactions? *Dev. Cell*. 23:11–20. http://dx.doi.org/10.1016/j.devcel.2012.06.012

Couet, J., M. Sargiacomo, and M.P. Lisanti. 1997. Interaction of a receptor tyrosine kinase, EGF-R, with caveolins. Caveolin binding negatively regulates tyrosine and serine/threonine kinase activities. *J. Biol. Chem.* 272:30429–30438. http://dx.doi.org/10.1074/jbc.272.48.30429

Diggle, P.J., J. Mateu, and H.E. Clough. 2000. A comparison between parametric and non-parametric approaches to the analysis of replicated spatial point patterns. *Adv. Appl. Probab.* 32:331–343. http://dx.doi.org/10.1239/aap/1013540166

Engelman, J.A., C. Chu, A. Lin, H. Jo, T. Ikezu, T. Okamoto, D.S. Kohtz, and M.P. Lisanti. 1998. Caveolin-mediated regulation of signaling along the p42/44 MAP kinase cascade in vivo. A role for the caveolin-scaffolding domain. *FEBS Lett.* 428:205–211. http://dx.doi.org/10.1016/S0014-5793(98)00470-0

Fairn, G.D., N.L. Schieber, N. Ariotti, S. Murphy, L. Kuerschner, R.I. Webb, S. Grinstein, and R.G. Parton. 2011. High-resolution mapping reveals topologically distinct cellular pools of phosphatidylserine. *J. Cell Biol.* 194:257–275. http://dx.doi.org/10.1083/jcb.201012028

Fernández, M.A., C. Albor, M. Ingelmo-Torres, S.J. Nixon, C. Ferguson, T. Kurzchalia, F. Tebar, C. Enrich, R.G. Parton, and A. Pol. 2006. Caveolin-1 is essential for liver regeneration. *Science*. 313:1628–1632. http://dx.doi.org/10.1126/science.1130773

Fernández-Rojo, M.A., M. Gongora, R.L. Fitzsimmons, N. Martel, S.D. Martin, S.J. Nixon, A.J. Brooks, M.P. Ikonomopoulou, S. Martin, H.P. Lo, et al. 2013. Caveolin-1 is necessary for hepatic oxidative lipid metabolism: evidence for crosstalk between caveolin-1 and bile acid signaling. *Cell Rep.* 4:238–247. http://dx.doi.org/10.1016/j.celrep.2013.06.017

Frank, P.G., M.W. Cheung, S. Pavlides, G. Llaverias, D.S. Park, and M.P. Lisanti. 2006. Caveolin-1 and regulation of cellular cholesterol homeostasis. *Am. J. Physiol. Heart Circ. Physiol.* 291:H677–H686. http://dx.doi.org/10.1152/ajpheart.01092.2005

Galbiati, F., D. Volonte, J.A. Engelman, G. Watanabe, R. Burk, R.G. Pestell, and M.P. Lisanti. 1998. Targeted downregulation of caveolin-1 is sufficient to drive cell transformation and hyperactivate the p42/44 MAP kinase cascade. *EMBO J.* 17:6633–6648. http://dx.doi.org/10.1093/emboj/17.22.6633

García-Cardeña, G., R. Fan, D.F. Stern, J. Liu, and W.C. Sessa. 1996. Endothelial nitric oxide synthase is regulated by tyrosine phosphorylation and interacts with caveolin-1. *J. Biol. Chem.* 271:27237–27240. http://dx.doi.org/10.1074/jbc.271.44.27237

Garofalo, T., L. Lenti, A. Longo, R. Misasi, V. Mattei, G.M. Pontieri, A. Pavan, and M. Sorice. 2002. Association of GM3 with Zap-70 induced by T cell activation in plasma membrane microdomains: GM3 as a marker of microdomains in human lymphocytes. *J. Biol. Chem.* 277:11233–11238. http://dx.doi.org/10.1074/jbc.M109601200

Gaus, K., S. Le Lay, N. Balasubramanian, and M.A. Schwartz. 2006. Integrin-mediated adhesion regulates membrane order. *J. Cell Biol.* 174:725–734. http://dx.doi.org/10.1083/jcb.200603034

Gorfe, A.A., M. Hanzal-Bayer, D. Abankwa, J.F. Hancock, and J.A. McCammon. 2007. Structure and dynamics of the full-length lipid-modified H-Ras protein in a 1,2-dimyristoylglycero-3-phosphocholine bilayer. *J. Med. Chem.* 50:674–684. http://dx.doi.org/10.1021/jm061053f

Grande-García, A., A. Echarri, J. de Rooij, N.B. Alderson, C.M. Waterman-Storer, J.M. Valdivielso, and M.A. del Pozo. 2007. Caveolin-1 regulates cell polarization and directional migration through Src kinase and Rho GTPases. *J. Cell Biol.* 177:683–694. http://dx.doi.org/10.1083/jcb.200701006

Hancock, J.F. 2003. Ras proteins: different signals from different locations. *Nat. Rev. Mol. Cell Biol.* 4:373–384. http://dx.doi.org/10.1038/nrm1105

Hancock, J.F., and R.G. Parton. 2005. Ras plasma membrane signalling platforms. *Biochem. J.* 389:1–11. http://dx.doi.org/10.1042/BJ20050231

Hancock, J.F., and I.A. Prior. 2005. Electron microscopic imaging of Ras signaling domains. *Methods*. 37:165–172. http://dx.doi.org/10.1016/j.ymeth.2005.05.018

Hao, M.M., and F.R. Maxfield. 2000. Characterization of rapid membrane internalization and recycling. *J. Biol. Chem.* 275:15279–15286. http://dx.doi.org/10.1074/jbc.275.20.15279

Hashiramoto, A., H. Mizukami, and T. Yamashita. 2006. Ganglioside GM3 promotes cell migration by regulating MAPK and c-Fos/AP-1. *Oncogene*. 25:3948–3955. http://dx.doi.org/10.1038/sj.onc.1209416

Hernández-Deviez, D.J., M.T. Howes, S.H. Laval, K. Bushby, J.F. Hancock, and R.G. Parton. 2008. Caveolin regulates endocytosis of the muscle repair protein, dysferlin. *J. Biol. Chem.* 283:6476–6488. http://dx.doi.org/10.1074/jbc.M708776200

Hibino, K., T.M. Watanabe, J. Kozuka, A.H. Iwane, T. Okada, T. Kataoka, T. Yanagida, and Y. Sako. 2003. Single- and multiple-molecule dynamics of the signaling from H-Ras to cRaf-1 visualized on the plasma membrane of living cells. *ChemPhysChem*. 4:748–753. http://dx.doi.org/10.1002/cphc.200300731

Hill, M.M., M. Bastiani, R. Luetterforst, M. Kirkham, A. Kirkham, S.J. Nixon, P. Walser, D. Abankwa, V.M. Oorschot, S. Martin, et al. 2008. PTRF-Cavin, a conserved cytoplasmic protein required for caveola formation and function. *Cell*. 132:113–124. http://dx.doi.org/10.1016/j.cell.2007.11.042

Hoffmann, C., A. Berking, F. Agerer, A. Buntru, F. Neske, G.S. Chhatwal, K. Ohlsen, and C.R. Hauck. 2010. Caveolin limits membrane microdomain mobility and integrin-mediated uptake of fibronectin-binding pathogens. *J. Cell Sci.* 123:4280–4291. http://dx.doi.org/10.1242/jcs.064006

Kay, J.G., M. Koivusalo, X. Ma, T. Wohland, and S. Grinstein. 2012. Phosphatidylserine dynamics in cellular membranes. *Mol. Biol. Cell*. 23:2198–2212. http://dx.doi.org/10.1091/mbc.E11-11-0936

Kuroda, S., T. Ohtsuka, B. Yamamori, K. Fukui, K. Shimizu, and Y. Takai. 1996. Different effects of various phospholipids on Ki-Ras-, Ha-Ras-, and Rap1B-induced B-Raf activation. *J. Biol. Chem.* 271:14680–14683. http://dx.doi.org/10.1074/jbc.271.25.14680

Li, S., J. Couet, and M.P. Lisanti. 1996. Src tyrosine kinases, Galpha subunits, and H-Ras share a common membrane-anchored scaffolding protein, caveolin. Caveolin binding negatively regulates the auto-activation of Src tyrosine kinases. *J. Biol. Chem.* 271:29182–29190. http://dx.doi.org/10.1074/jbc.271.46.29182

Lingwood, D., and K. Simons. 2010. Lipid rafts as a membrane-organizing principle. *Science*. 327:46–50. http://dx.doi.org/10.1126/science.1174621

Magalhães, A., J. Gomes, M.N. Ismail, S.M. Haslam, N. Mendes, H. Osório, L. David, J. Le Pendu, R. Haas, A. Dell, et al. 2009. Fut2-null mice display an altered glycosylation profile and impaired BabA-mediated Helicobacter pylori adhesion to gastric mucosa. *Glycobiology*. 19:1525–1536. http://dx.doi.org/10.1093/glycob/cwp131

Marcos, N.T., A. Magalhães, B. Ferreira, M.J. Oliveira, A.S. Carvalho, N. Mendes, T. Gilmartin, S.R. Head, C. Figueiredo, L. David, et al. 2008. Helicobacter pylori induces beta3GnT5 in human gastric cell lines,

Downloaded from http://rupress.org/jcb/article-pdf/204/5/777/1583044/jcb_201307055.pdf by guest on 24 April 2024

modulating expression of the SabA ligand sialyl-Lewis x. *J. Clin. Invest.* 118:2325–2336.

Murakoshi, H., R. Iino, T. Kobayashi, T. Fujiwara, C. Ohshima, A. Yoshimura, and A. Kusumi. 2004. Single-molecule imaging analysis of Ras activation in living cells. *Proc. Natl. Acad. Sci. USA*. 101:7317–7322. http://dx.doi.org/10.1073/pnas.0401354101

Murata, M., J. Peränen, R. Schreiner, F. Wieland, T.V. Kurzchalia, and K. Simons. 1995. VIP21/caveolin is a cholesterol-binding protein. *Proc. Natl. Acad. Sci. USA*. 92:10339–10343. http://dx.doi.org/10.1073/pnas.92.22.10339

Ortegren, U., M. Karlsson, N. Blazic, M. Blomqvist, F.H. Nystrom, J. Gustavsson, P. Fredman, and P. Strålfors. 2004. Lipids and glycosphingolipids in caveolae and surrounding plasma membrane of primary rat adipocytes. *Eur. J. Biochem.* 271:2028–2036. http://dx.doi.org/10.1111/j.1432-1033.2004.04117.x

Parton, R.G., and M.A. del Pozo. 2013. Caveolae as plasma membrane sensors, protectors and organizers. *Nat. Rev. Mol. Cell Biol.* 14:98–112. http://dx.doi.org/10.1038/nrm3512

Parton, R.G., and K. Simons. 2007. The multiple faces of caveolae. *Nat. Rev. Mol. Cell Biol.* 8:185–194. http://dx.doi.org/10.1038/nrm2122

Pettitt, T.R., M. McDermott, K.M. Saqib, N. Shimwell, and M.J. Wakelam. 2001. Phospholipase D1b and D2a generate structurally identical phosphatidic acid species in mammalian cells. *Biochem. J.* 360:707–715. http://dx.doi.org/10.1042/0264-6021:3600707

Plowman, S.J., C. Muncke, R.G. Parton, and J.F. Hancock. 2005. H-ras, K-ras, and inner plasma membrane raft proteins operate in nanoclusters with differential dependence on the actin cytoskeleton. *Proc. Natl. Acad. Sci. USA*. 102:15500–15505. http://dx.doi.org/10.1073/pnas.0504114102

Plowman, S.J., N. Ariotti, A. Goodall, R.G. Parton, and J.F. Hancock. 2008. Electrostatic interactions positively regulate K-Ras nanocluster formation and function. *Mol. Cell. Biol.* 28:4377–4385. http://dx.doi.org/10.1128/MCB.00050-08

Prinetti, A., M. Aureli, G. Illuzzi, S. Prioni, V. Nocco, F. Scandroglio, N. Gagliano, G. Tredici, V. Rodriguez-Menendez, V. Chigorno, and S. Sonnino. 2010. GM3 synthase overexpression results in reduced cell motility and in caveolin-1 upregulation in human ovarian carcinoma cells. *Glycobiology*. 20:62–77. http://dx.doi.org/10.1093/glycob/cwp143

Prior, I.A., A. Harding, J. Yan, J. Sluimer, R.G. Parton, and J.F. Hancock. 2001. GTP-dependent segregation of H-ras from lipid rafts is required for biological activity. *Nat. Cell Biol.* 3:368–375. http://dx.doi.org/10.1038/35070050

Prior, I.A., C. Muncke, R.G. Parton, and J.F. Hancock. 2003a. Direct visualization of Ras proteins in spatially distinct cell surface microdomains. *J. Cell Biol.* 160:165–170. http://dx.doi.org/10.1083/jcb.200209091

Prior, I.A., R.G. Parton, and J.F. Hancock. 2003b. Observing cell surface signaling domains using electron microscopy. *Sci. STKE*. 2003:PL9.

Pyne, S., K.C. Kong, and P.I. Darroch. 2004. Lysophosphatidic acid and sphingosine 1-phosphate biology: the role of lipid phosphate phosphatases. *Semin. Cell Dev. Biol.* 15:491–501. http://dx.doi.org/10.1016/j.semcdb.2004.05.007

Rotblat, B., I.A. Prior, C. Muncke, R.G. Parton, Y. Kloog, Y.I. Henis, and J.F. Hancock. 2004. Three separable domains regulate GTP-dependent association of H-ras with the plasma membrane. *Mol. Cell. Biol.* 24:6799–6810. http://dx.doi.org/10.1128/MCB.24.15.6799-6810.2004

Rothberg, K.G., J.E. Heuser, W.C. Donzell, Y.S. Ying, J.R. Glenney, and R.G. Anderson. 1992. Caveolin, a protein component of caveolae membrane coats. *Cell*. 68:673–682. http://dx.doi.org/10.1016/0092-8674(92)90143-Z

Roy, S., R. Luetterforst, A. Harding, A. Apolloni, M. Etheridge, E. Stang, B. Rolls, J.F. Hancock, and R.G. Parton. 1999. Dominant-negative caveolin inhibits H-Ras function by disrupting cholesterol-rich plasma membrane domains. *Nat. Cell Biol.* 1:98–105. http://dx.doi.org/10.1038/15687

Roy, S., S. Plowman, B. Rotblat, I.A. Prior, C. Muncke, S. Grainger, R.G. Parton, Y.I. Henis, Y. Kloog, and J.F. Hancock. 2005. Individual palmitoyl residues serve distinct roles in H-ras trafficking, microlocalization, and signaling. *Mol. Cell. Biol.* 25:6722–6733. http://dx.doi.org/10.1128/MCB.25.15.6722-6733.2005

Sandhoff, K., and T. Kolter. 2003. Biosynthesis and degradation of mammalian glycosphingolipids. *Philos. Trans. R. Soc. Lond. B Biol. Sci.* 358:847–861. http://dx.doi.org/10.1098/rstb.2003.1265

Sinha, B., D. Köster, R. Ruez, P. Gonnord, M. Bastiani, D. Abankwa, R.V. Stan, G. Butler-Browne, B. Vedie, L. Johannes, et al. 2011. Cells respond to mechanical stress by rapid disassembly of caveolae. *Cell*. 144:402–413. http://dx.doi.org/10.1016/j.cell.2010.12.031

Suzuki, Y., K. Hidari, M. Matsumoto, M. Ikeda, and N. Tsuchida. 1989. Altered ganglioside expression in ras-oncogene-transformed cells. *J. Biochem.* 106:34–37.

Tian, T., A. Harding, K. Inder, S. Plowman, R.G. Parton, and J.F. Hancock. 2007. Plasma membrane nanoswitches generate high-fidelity Ras signal transduction. *Nat. Cell Biol.* 9:905–914. http://dx.doi.org/10.1038/ncb1615

van der Hoeven, D., K.J. Cho, X. Ma, S. Chigurupati, R.G. Parton, and J.F. Hancock. 2013. Fendiline inhibits K-Ras plasma membrane localization and blocks K-Ras signal transmission. *Mol. Cell. Biol.* 33:237–251. http://dx.doi.org/10.1128/MCB.00884-12

Wanaski, S.P., B.K. Ng, and M. Glaser. 2003. Caveolin scaffolding region and the membrane binding region of SRC form lateral membrane domains. *Biochemistry*. 42:42–56. http://dx.doi.org/10.1021/bi012097n

Wang, X.Q., P. Sun, and A.S. Paller. 2002. Ganglioside induces caveolin-1 redistribution and interaction with the epidermal growth factor receptor. *J. Biol. Chem.* 277:47028–47034. http://dx.doi.org/10.1074/jbc.M208257200

Yamamoto, K., and J. Ando. 2013. Endothelial cell and model membranes respond to shear stress by rapidly decreasing the order of their lipid phases. *J. Cell Sci.* 126:1227–1234. http://dx.doi.org/10.1242/jcs.119628

Yamashita, T., A. Hashiramoto, M. Haluzik, H. Mizukami, S. Beck, A. Norton, M. Kono, S. Tsuji, J.L. Daniotti, N. Werth, et al. 2003. Enhanced insulin sensitivity in mice lacking ganglioside GM3. *Proc. Natl. Acad. Sci. USA*. 100:3445–3449. http://dx.doi.org/10.1073/pnas.0635898100

Zhou, Y., S.J. Plowman, L.M. Lichtenberger, and J.F. Hancock. 2010. The anti-inflammatory drug indomethacin alters nanoclustering in synthetic and cell plasma membranes. *J. Biol. Chem.* 285:35188–35195. http://dx.doi.org/10.1074/jbc.M110.141200

Zhou, Y., K.J. Cho, S.J. Plowman, and J.F. Hancock. 2012. Nonsteroidal anti-inflammatory drugs alter the spatiotemporal organization of Ras proteins on the plasma membrane. *J. Biol. Chem.* 287:16586–16595. http://dx.doi.org/10.1074/jbc.M112.348490

Downloaded from http://rupress.org/jcb/article-pdf/204/5/777/1583044/jcb_201307055.pdf by guest on 24 April 2024